

Review

Preparation and Real World Applications of Titania Composite Materials for Photocatalytic Surface, Air, and Water Purification: State of the Art

Volker Seiß , Susanne Thiel  and Maik Eichelbaum * 

Department of Applied Chemistry, Georg Simon Ohm University of Applied Sciences Nuremberg, Prinzregentenauer 47, 90489 Nürnberg, Germany

* Correspondence: maik.eichelbaum@th-nuernberg.de; Tel.: +49-911-5880-1561

Abstract: The semiconducting transition metal oxide TiO_2 is a rather cheap and non-toxic material with superior photocatalytic properties. TiO_2 thin films and nanoparticles are known to have antibacterial, antiviral, antifungal, antialgal, self, water, and air-cleaning properties under UV or sun light irradiation. Based on these excellent qualities, titania holds great promises in various fields of applications. The vast majority of published field and pilot scale studies are dealing with the modification of building materials or generally focus on air purification. Based on the reviewed papers, for the coating of glass, walls, ceilings, streets, tunnels, and other large surfaces, titania is usually applied by spray-coating due to the scalability and cost-efficiency of this method compared to alternative coating procedures. In contrast, commercialized applications of titania in medical fields or in water purification are rarely found. Moreover, in many realistic test scenarios it becomes evident that the photocatalytic activity is often significantly lower than in laboratory settings. In this review, we will give an overview on the most relevant real world applications and commonly applied preparation methods for these purposes. We will also look at the relevant bottlenecks such as visible light photocatalytic activity and long-term stability and will make suggestions to overcome these hurdles for a widespread usage of titania as photocatalyst.

Keywords: TiO_2 photocatalysis; semiconductor thin films; antiviral and antibacterial properties; air purification; water purification; easy-to-clean effect; disinfection



Citation: Seiß, V.; Thiel, S.; Eichelbaum, M. Preparation and Real World Applications of Titania Composite Materials for Photocatalytic Surface, Air, and Water Purification: State of the Art. *Inorganics* **2022**, *10*, 139. <https://doi.org/10.3390/inorganics10090139>

Academic Editors: Alejandro Pérez-Larios and Oomman K. Varghese

Received: 10 August 2022

Accepted: 9 September 2022

Published: 15 September 2022

Publisher's Note: MDPI stays neutral with regard to jurisdictional claims in published maps and institutional affiliations.



Copyright: © 2022 by the authors. Licensee MDPI, Basel, Switzerland. This article is an open access article distributed under the terms and conditions of the Creative Commons Attribution (CC BY) license (<https://creativecommons.org/licenses/by/4.0/>).

1. Introduction

If nothing else, the Corona pandemic demonstrated the importance of antimicrobial surfaces, clean air, and germ-free water [1,2]. Access to drinking water free of disease-causing viruses, bacteria, and further organic and inorganic pollutants still poses a major challenge in many regions in the world, especially in developing countries. A growing population and climate change are exacerbating this problem [3–6]. One way to tackle these challenges is water purification by the photocatalytic oxidation of organic and biologic pollutants [7,8]. E.g., TiO_2 on PET has been used for water treatment or on membranes for oil-water separation as well as for self-cleaning of the membrane [9,10]. Photocatalysis can also be used to remove antibiotics or pharmaceutically active compounds from water [11,12]. Photocatalysts are also being tested for air purification applications [13,14]. One major source of concern is the nitrogen oxide concentration in the air of urban areas. Here, so-called photoactive building materials such as paving stones, roof tiles or concrete walls for road tunnels are currently being developed and tested, which can oxidize the gaseous NO_x contaminant to water soluble nitrates [15–17]. Photocatalytically active building material surfaces are also expected to contribute to the degradation of a number of other inorganic and organic pollutants such as sulfur oxides, volatile organic compounds, and ozone [18–20]. In addition, the risk of microbial infestation of photocatalytic building materials by algae, fungi, or lichens is significantly reduced or they are generally easier

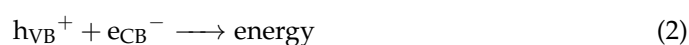
to clean (“easy-to-clean effect”) [19,21]. Window glass surfaces coated with a transparent photocatalyst film can exhibit very good anti-fogging and self-cleaning properties under UV irradiation due to the formation of amphiphilic (i.e., combined hydrophilic and oleophilic) and super-hydrophilic domains [22,23]. The photocatalytic properties of coatings and admixtures could also be useful in the field of interior paints and plasters, since typical indoor pollutants such as formaldehyde and acetaldehyde, as well as odors such as cigarette smoke or cooking fat fumes, can be converted into harmless or odorless compounds by photoactive surfaces. The antimicrobial effect of photoactive interior wall paints/plasters can also prevent or reduce possible mold infestation. The air-purifying effect and odor neutralization can be used, among other things, in filter systems, air-conditioning systems or in the catering industry [13,14,24–26]. And finally, antimicrobial photocatalytic coatings are important in the fields of medical technology, household appliances, textiles, and other hygiene areas [27–30].

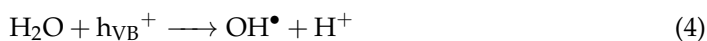
The term “photocatalysis” has been coined for various, often very different reaction schemes. As a consequence, when the term is used in the scientific literature, it is not always clear which exact mechanism is actually meant in each specific case. IUPAC defines “photocatalysis” as a “[c]atalytic reaction involving light absorption by a catalyst or by a substrate” [31]. However, in this definition important distinguishing features are missing. Moreover, “light” is an additional “catalytic” parameter that might contradict Ostwald’s original definition of catalysis, which says that a catalyst is not to appear in the final product of a chemical reaction. Therefore, in 1983, Salomon suggested to differentiate between reactions with catalytically active photons (i.e., quantum yield > 1), called photogenerated catalysis, and with non-catalytic photons (i.e., quantum yield < 1), which he called catalyzed photolysis [32]. The latter term was further classified into many more reactions schemes, whose description would go far beyond the scope of this review. As for reactions with photons on a heterogeneous semiconductor such as titania, the term “semiconductor-assisted photoreaction” should be most appropriate as suggested by Serpone and Emeline, since photons are consumed stoichiometrically rather than act as (non-consumed) “catalytic” photons [33]. However, since the term “photocatalysis” is overwhelmingly used in the scientific community in terms of an acceleration of a photoreaction by a catalyst (without having in mind any mechanistic implications), we will also use this word in this sense in our review.

The semiconductor-assisted photoreaction mechanism responsible for the abatement of most of the pollutants by oxidation upon irradiation with UV or visible light can be generally described by some peculiar basic mechanisms. The most important underlying reactions are schematically shown in Figure 1 and have been described in detail in other reviews (e.g., in Refs. [34–36]). If a photoconductor is radiated with energy equal or higher than the energy of the band gap, an electron is excited from the valence band (VB) into the conduction band (CB) (Equation (1)).



In consequence, a positive hole is generated in the valence band. Subsequently, charge carrier recombination (Equation (2)), diffusion, and surface reactions are possible consecutive pathways. Photogenerated electrons trapped at surface states may react with molecular oxygen (Equation (3)), while holes trapped at surface states can react with water (Equation (4)). As typical products superoxide radicals ($\text{O}_2^{\bullet-}$) and hydroxyl radicals (OH^\bullet) have been observed.





Finally, due to the high standard reduction potential of the photogenerated radicals, pollutants are effectively oxidized and hence degraded. In the following, some likely consecutive reactions are summarized:

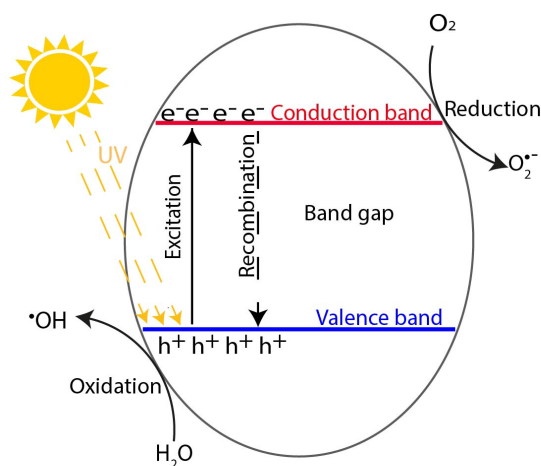
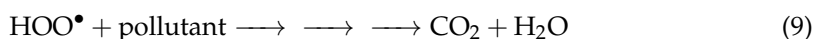
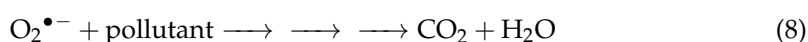
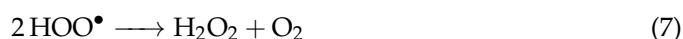
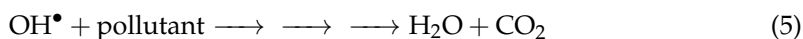


Figure 1. Principle mechanisms for charge carrier generation and consecutive reactions in a photocatalytically active semiconductor during irradiation.

The probably most promising candidate for such photocatalytic applications is titanium dioxide (or titania, TiO_2) due to its high exciton binding energy, its insolubility in aqueous liquids, its chemical and biological inertness and photostability. Moreover, it is not toxic, relatively cheap, and abundant. The crystalline modifications of titania anatase and rutile are most often utilized in photocatalytic applications with corresponding band gaps of 3.2 and 3.0 eV, respectively [36–38]. Rarely, the modification brookite with a band gap of 3.2 eV has also been used as photocatalyst [36,39].

Several analytical techniques have been established for the analysis of the photocatalytic effect. E.g., the degradation of methylene blue or methyl orange is a standard method for measuring the activity of the photocatalyst in contact with a liquid [27,40–42]. In addition, the direct testing of bacterial inactivation is also conceivable, as was probably first described by Matsunaga et al. [43]. Furthermore, very often NO_x or volatile organic compounds (VOC) have been used as real or model pollutants for the determination of the activity of a photocatalyst in air [16,25]. In addition, sophisticated analytical methods can directly determine mechanistic aspects such as degradation reaction mechanisms, charge carrier excitation, recombination, diffusion, and other associated processes. Electrochemical methods such as (photo)impedance spectroscopy, linear sweep voltammetry, (chopped light) chronoamperometry, and intensity modulated photocurrent and photovoltage spectroscopy have to be mentioned here [27,40]. Recently, Seiß et al. could show

that photoelectrochemically deduced parameters such as charge transfer efficiency and photoquantum yield can be quite well correlated with photocatalytic kinetics comprising the methylene blue degradation rate and bacterial survival rate for different titania thin films on glass (Figure 2) [27].

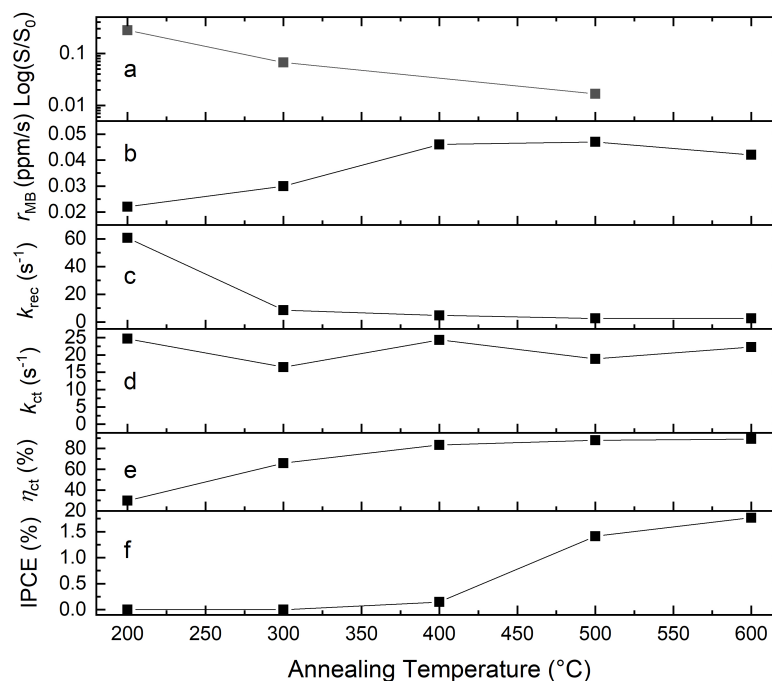


Figure 2. Comparison of photocatalytic and photoelectrochemical parameters of TiO_2 films annealed at different temperatures on FTO glass under UV-A irradiation: (a) *E. coli* survival rate after 60 min irradiation (please note, that the data point at “200 °C” denotes here an uncoated glass reference sample), (b) methylene blue degradation rate, (c) charge carrier recombination rate, (d) charge transfer rate, (e) charge transfer efficiency, and (f) photoquantum yield IPCE (incident photon conversion efficiency). The electrochemical parameters were determined at a potential of approximately $-0.6 \text{ V}_{\text{Ag}/\text{AgCl}}$. (Reprinted/adapted with permission from Ref. [44]). More information can be found in Ref. [27].

Moreover, photoluminescence spectroscopy and the associated lifetime analysis of photogenerated charge carriers is another valuable method [45–47]. The German Fraunhofer Institute for Surface Engineering and Thin Films IST has developed a measuring method in which a polymer film with a dye monolayer is clamped into a mobile device and pressed onto a potentially photocatalytic surface. The photoactivity is determined qualitatively and quantitatively via the decay of the dye luminescence upon irradiation. The method is fast, mobile and creates comparable conditions between different samples [48]. However, the overwhelming part of the published results on the in-depth analysis of photocatalytic properties comprehends samples in the research state rather than composites in real applications. For the latter, an insightful discussion of the photocatalytic properties is very often missing.

Due to the low photocatalytic efficiency in visible light, the low quantum efficiency in composite materials due to rather high charge carrier recombination rates, and rather short durability in harsh (ambient) environments, photocatalysts are still rarely used in real world applications [14,34–36,49–51]. Moreover, general nanoparticle toxicity issues [52,53] and the additional steps required for the separation of the photocatalyst in water purification applications face an additional problem making them still not very competitive to alternative methods [7,54]. Titania coatings or immobilized nanoparticles are possible alternatives for suspended powders to avoid the separation problem in water purification

systems [55]. Thin films are generally the method of choice for air purification applications. Possible routes for the production of thin TiO₂ films and for the immobilization of TiO₂ nanoparticles on a surface are sol-gel methods with spin or dip coating, chemical and physical vapor deposition or spray coating of a sol or of nanoparticles in a solution or suspension [56]. For the coating of large glass areas the so called slot-die process has been applied [57].

The aim of this review is to give a pointed overview on already existent synthesis routes, deposition methods, and applications with a special focus on commercialized applications of titania composite systems or at least on research results in a very advanced stage of development with proven photocatalytic performance. We will also discuss the-to our mind-most relevant pitfalls that are preventing a widespread usage of photocatalytic materials so far, and how to deal with these challenges. The review is intended to provide an impression on the current state of the field and upcoming developments. We do not claim a complete coverage of all ever published findings and we always refer to the relevant source for an accurate representation of the respective cited research results.

2. Band Gap Engineering

Crystalline TiO₂ (as rutile, anatase or brookite) can absorb only about 4% of the solar energy due to its large band gap in the range of 3.0–3.2 eV. As a consequence, the true incident photon conversion yield of most sun-light and semiconductor-assisted photoreactions is low. The aim of exploiting visible light can be achieved by applying various techniques such as doping or modification with metals and non-metals, coupling of semiconductors, or dye sensitization [36]. Since only the former technique seems to allow cost-efficient and robust synthesis routes for realistic applications of titania coatings, this chapter will concentrate on metal and non-metal doping.

Different doping methods to improve the photocatalytic properties under visible light have already been reviewed, e.g., by Pelaez et al. [36], Li et al. [58], Nasr et al. [59], and Wang et al. [60]. In our review, we will repeat the most relevant concepts for a better understanding of the applications presented in the following chapters. We will hence concentrate on dopants and modifications that are of practical relevance so far.

2.1. Metal Doping

Noble metals such as Au, Ag, Pd, or Pt as well as transition metals such as V, Cr, Fe, Co, Cu, Mo, Ni, and Zn were used to dope titania and improve its absorption of visible light [40,47,61–66]. Doping with noble metals can both enable absorption of longer wavelengths and improve charge carrier separation [67–69]. This is achieved by the circumstance that the Fermi levels of the doped metals are localized below the conduction band of the TiO₂. By metal doping, Schottky barriers can form at the TiO₂-metal interface, which behave like electron traps. The photoexcited electrons migrate from the TiO₂ to the metal through the Schottky barrier until the Fermi levels are equalized, while the photogenerated holes remain in the TiO₂. This effect improves charge separation and results in a lower electron-hole recombination [70,71].

The absorption of longer wavelengths due to noble metal doping is usually associated with the effect of surface plasmon resonance. Surface plasmons are caused by a collective oscillation of free charge carriers on the surface of conducting materials upon interaction with light (Figure 3). Resonance occurs when the particles are irradiated with light corresponding to their plasmon frequency, resulting in induced electric fields on the surface of the particles. Regarding the generated electric fields, it was shown that the generated electric fields can lead to a one thousand times larger charge carrier formation compared to the incident electric field. The plasmon frequency can be highly influenced and depends on factors such as nanoparticle material, size, and shape [72].

The positive influence of noble metal doping on charge separation in titania was proven, e.g., in the removal of *Mycobacterium tuberculosis*. Here, HEPA filter were coated with silver-doped TiO₂. Due to the doping, a complete removal of *M. tuberculosis* was

achieved after only 100 min, while undoped TiO_2 required about 180 min for a complete removal. A concentration dependence was also observed, suggesting that an excessively high concentration of Ag leads to increased recombination, since Ag becomes the recombination center [62].

The absorption of longer wavelengths due to the surface plasmon resonance effect was shown by doping of TiO_2 with Au. Here, enhanced absorption was measured at wavelengths of about 500 nm. Results from emission photoluminescence spectra indicated that additional energy levels are present at 2.7 eV and 2.54 eV, which were assigned to oxygen vacancy states. In addition, emission photoluminescence spectra results refer to a lower recombination of the Au doped samples compared to pure TiO_2 . Both effects led to higher photoactivity in the degradation of Rhodamine B under simulated solar light for Au doped TiO_2 as compared to the undoped sample [47].

By doping TiO_2 with Pd, the band gap could be decreased from 3.2 eV for pure TiO_2 to 3.07 eV for the highest Pd concentration. It was observed that with increasing Pd concentration the band gap got smaller. Doping with Pd at various concentrations resulted in higher photoactivity under UV irradiation compared to pure TiO_2 . Regarding the concentration, it was measured that the photoactivity increases up to a limiting concentration and finally decreases with increasing concentration. It was concluded that excess doping leads to a conglomeration of Pd particles, which then act as recombination centers [40].

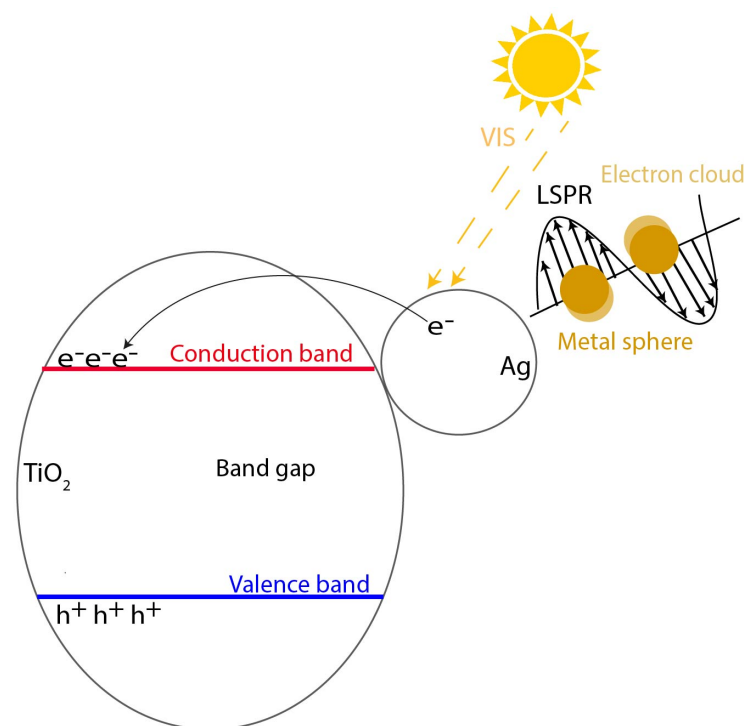


Figure 3. Schematic representation of the surface plasmon resonance (SPR) effect of silver doped TiO_2 .

Doping with transition metals can also positively influence the photoactivity of TiO_2 . Doping with Fe results in an $\text{Fe}^{3+}/\text{Fe}^{4+}$ energy level above the valence band of TiO_2 and an $\text{Fe}^{3+}/\text{Fe}^{2+}$ energy level located below the conduction band (Figure 4). This allows the material to absorb photons at wavelengths > 400 nm. Electrons can be photoexcited from the Fe^{3+} interband state (which generates Fe^{4+}) to the conduction band of TiO_2 . Fe^{3+} can serve both as hole or electron trap, since both resulting oxidation states of Fe^{4+} and Fe^{2+} can be formed. According to crystal field theory, Fe^{2+} and Fe^{4+} are relatively unstable as compared to Fe^{3+} , which has half-filled 3d orbitals. Therefore, charge transfer from Fe^{4+} and Fe^{2+} , respectively, to reaction species in air or water is preferred (Figure 4). Thus, doping with Fe^{3+} can cause a better (and faster) charge separation. However, Fe^{3+} can also become a recombination center, if the concentration of the ions is too high, leading

to a decrease in photoactivity [73,74]. The influence of Fe doping on the photocatalytic properties of P25 was studied upon the decomposition of acetaldehyde. It was found that the band gap decreased with increasing Fe content and was only 2.3 eV for an Fe content of 1.8 wt%. Under visible light irradiation, up to 65% of acetaldehyde could be removed after 1050 min for the Fe doped samples, while pure TiO₂ could only remove 40% of acetaldehyde. It is worth mentioning that the highest decomposition rate was observed for the lowest Fe concentration and the photoactivity declined with increasing Fe concentration. It was concluded that the higher Fe content increased the recombination, which resulted in lower photoactivity [63].

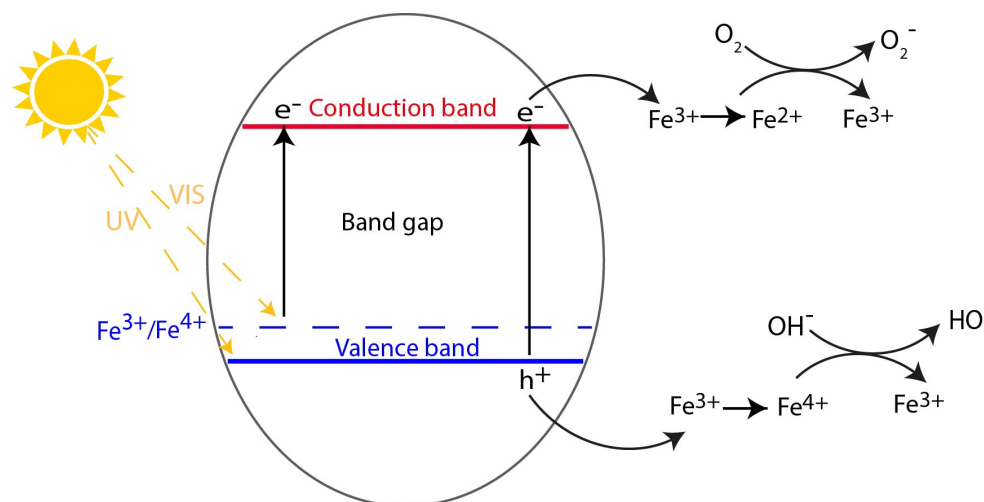


Figure 4. Energy diagram for doping with iron and possible consecutive reaction mechanisms under UV and visible light irradiation.

Also Cu and Mn doping was studied. When titania thin films are doped with Mn or Cu, an improvement in photocatalytic properties was observed with Mn doping, while a decline was observed for Cu doping. Since the photocatalytic properties depended on the Mn and Cu concentration, it was assumed that the Cu concentration was already too high for an improved activity. At low concentrations, the metals seem to contribute to lower recombination, while at high concentration they become recombination centers. Doping with Mn also improved the antibacterial properties compared to pure TiO₂ [64].

2.2. Non-Metal Doping

Doping with non-metals has mainly been carried out with N, S, C, and B [75–79]. The resulting properties vary depending on whether the non-metals are substitutional for oxygen or are incorporated as interstitial atoms. It is assumed that the substitution of oxygen mainly affects the valence band, which is built of O 2p states, yet there seem to be exceptions such as doping with fluorine. Here, the excess electron is lifted into the empty titanium levels and trapped in the Ti 3d orbital, which lies below the conduction band. Doping with lighter elements than oxygen such as N, C, and B causes the valence band to be depleted by one to three electrons depending on which element was used. It can be seen that the lower the atomic number, the higher the energy of the 2p levels. Figure 5 shows that the energy of the 2p states is increasing in the order of N, C, and B. The B 2p state has the highest energy level which leads to a smaller band gap [75].

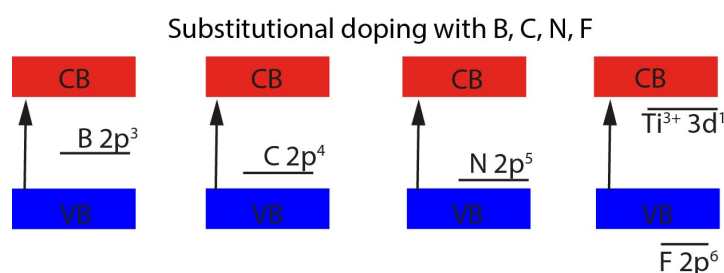


Figure 5. Schematic representation of the energy levels for substitutional doping in TiO_2 .

In contrast, the very small non-metal atoms can also diffuse through the interstitial spaces and bind to interstitial atoms. Depending on the redox potential of the doped element, they can be oxidized. For example, B gives up all three valence electrons to Ti interstitial ions, which is why three Ti^{3+} ions are formed. The boron atom is now bound to either 3 or 4 oxygen atoms, the three new B-O levels are below the valence band while the Ti^{3+} levels are below the conduction band [75,76] (Figure 6). The interstitial carbon atom has a higher electronegativity compared to B, which is why C only gives up two of the four valence electrons. This leads to the formation of two Ti^{3+} species, which are located below the conduction band. The levels of the three C-O bonds are below the valence band, while the additional C 2p pair is located in the band gap [75,76]. Nitrogen as a doping element is found to preferentially bind only one interstitial oxygen. The N atom pushes the oxygen atoms out of the Ti-O-Ti plane towards the interstitial space, resulting in an NO species with two additional electrons. Thus, it binds to the interstitial Ti with the π bonding system. As shown in Figure 6, the π NO states are below the valence band, while the π^* NO states are within the band gap [75,76]. In order to study the influence of N, single wall TiO_2 -carbon nanotubes (SWCNT) were doped with N. As a result, the methyl orange degradation under visible light was increased from about 40% for pure TiO_2 to about 72% for the doped material. Without the SWCNT as substrates, the degradation was at 50% [77].

The co-doping of N and F resulted in a higher activity for the methylene blue degradation under visible light than for the doping with N only. With increasing F content, an additionally improved photoactivity could be measured. From the results of XRD and absorption spectra, it was concluded that doping with F prevents the growth of TiO_2 particles and enhances the absorption in the visible range [79].

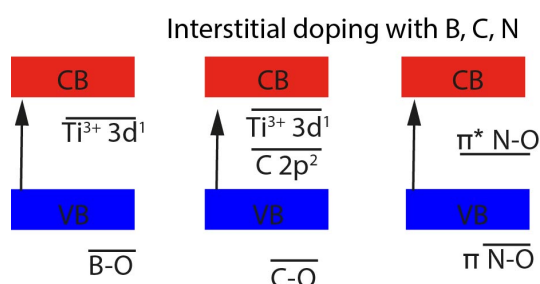


Figure 6. Schematic representation of the energy levels for interstitial doping in TiO_2 .

Fan et al. doped TiO_2 with C which shifted the onset of the absorption curve of the doped sample to about 700 nm. The doped TiO_2 was able to degrade 60% of the methyl orange ($\lambda > 400$ nm) in a test after half an hour, while the undoped TiO_2 showed negligible degradation.

Our literature survey exhibited that doping and co-doping techniques are increasingly used in real applications. The doping with noble metals is obviously in many cases too expensive to manufacture coatings or admixtures on large scales and is hence rarely applied. In contrast, non-metals such as carbon are much more suitable. One interesting application of a carbon-doped titania is asphalt coating. The doped sample showed a

complete degradation of NO_x in a confined environment after 90 min. For undoped TiO_2 , the NO_x concentration was still at about 70% after 90 min. The sample was irradiated with a solar spectrum lamp. It was observed that the photoactivity also increased with increasing dopant concentration [78]. More applications are to be discussed in the respective sections below.

3. Synthesis and Preparation

For practical applications it is usually inevitable to utilize the photocatalyst in the form of thin films or nanoparticles that are immobilized on substrates. There are multiple ways to deposit titanium dioxide layers on different supports. In principle, four routes can be distinguished, which are summarized in Figure 7: (A) Titanium dioxide can be deposited as homogeneous film [47,80–82]. (B) Another way is to incorporate titanium dioxide nanoparticles directly into the material of the substrate [83,84]. (C) Alternatively, titania nanoparticles can be directly applied to a surface. (D) Another common method is to suspend P25 from former Degussa (now Evonik), CristalACTIV™ PC500, or a comparable crystalline titania powder in, e.g., water, resin or a sol and then coat it onto a surface. It is also possible to coat the surface with silica beforehand or to add a binder such as ethylene glycol or a silane to the suspension. Titanium dioxide can also be incorporated into paint as a stabilizer and then be coated onto a surface [25,62,85–93].

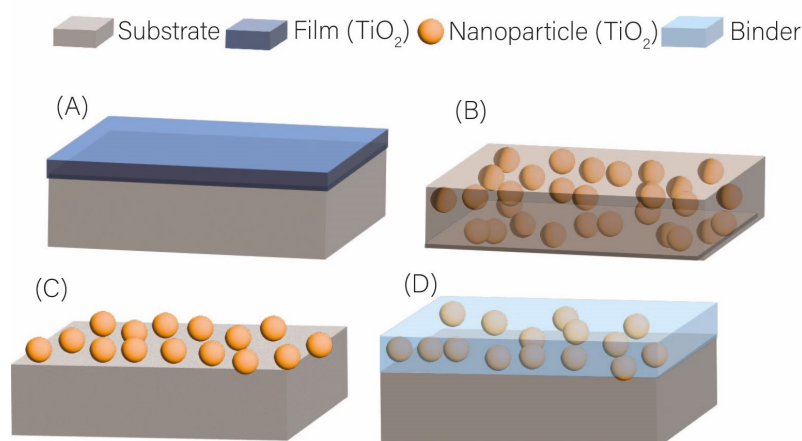


Figure 7. Multiple ways for preparation of titania at surfaces: Homogeneous TiO_2 film (A), titania nanoparticles suspended in substrate (B), titania nanoparticles directly applied to the surface (C), and titania nanoparticles in a coating layer (D).

Based on these basic preparation routes, the to our mind most practically relevant synthesis routes will be described in detail in the following paragraphs. There are several other ways to produce and coat titanium dioxide [56]. Here, however, we will restrict this review to those ways that prove to be of practical relevance. Please note that not all syntheses used in practical applications can be listed here due to secrecy issues of commercial applications or simply due to a lack of openly published information.

3.1. Dip and Spin Coating, Immersion, and Impregnation of Sol-Gel and TiO_2 Suspensions

In the dip coating process, a substrate (or generally the to be coated material) is simply immersed in a solution or suspension containing the coating material. Nanoparticles or the sol in the solution or suspension ideally adhere to the surface of the substrate. Then, the substrate is pulled out of the solution or suspension in a controlled manner. The particular advantages are the simplicity of this method, and its reliability, low costs, relative independence from the substrate used and the possibility to coat even geometrically complex materials [56]. Even monolithic cellulose acetate, fibres, membranes, or other small components were successfully dip coated by a suspension of P25 or other nanoparti-

cles [62,87,89,93–96]. In addition, membranes and monoliths were coated by immersion in a sol or gel of titania [86,97–99]. Moreover, the synthesis route via sol-gel with alkoxides is described as significantly cheaper compared to physical and other chemical deposition methods [100,101].

Thunyasirion et al. tested three different binders to enhance the adherence of the nanoparticles to the substrate (glass fiber), namely polyethylene glycol, silane and DURAMAX™ in combination with aqueous suspensions of P25. DURAMAX™ turned out to be the most efficient binder [62].

Rodrigues-Silva et al. synthesized a sol, aged it to a gel, which they then diluted and immersed in cellulose acetate monoliths [97]. For the synthesis, they used just titanium butoxide TOBT (Figure 8), ethanol, water and acetic acid. An anatase morphology was obtained.

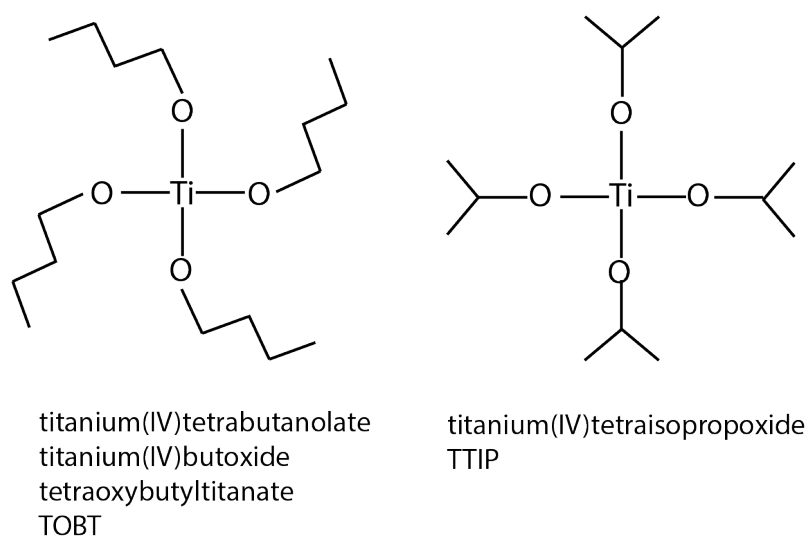


Figure 8. Common titania sol-gel precursors.

Moustakas et al. synthesized a sol in which they immersed a membrane [98]. For the synthesis of the sol, they used TOBT, water and nitric acid, 1-propanol and, after ageing, urea. The obtained N-titania was of anatase modification.

Fazzani et al. immersed ceramized fabrics in either a sol consisting of diluted TiO_2 sol (commercially available) or in a sol consisting of diluted and SiO_2 -added TiO_2 sol [87]. The produced titania had a mixed anatase/rutile(16%) modification.

Porley et al. prepared a sol via TOBT, n-butanol and hydrochloric acid, to which they added P25 [86]. They then immersed glass spheres and tempered the sol at 500 °C. Some of the coated beads were modified. To do this, the spheres were placed several times in a bath of $\text{Bi}(\text{NO}_3)_3$ or KBr. In between, the spheres were rinsed with water and after repeated coating, they were annealed at 600 °C for 1 h.

Triton X-100 and water were mixed with cyclohexane by Ho [102]. After stirring, this mixture was added to TTIP (Figure 8) and stirred again. A ceramic was dipped into the resulting reverse micellar solution. The ceramic and the sol on the surface were then annealed at 500 °C to obtain anatase structure.

The spin coating process is very similar to dip coating. Here, a substrate is rotated and the solution or suspension with the sol-gel is dropped onto the substrate during spinning [56]. E.g., typically glass slides are coated with nanoparticles (or a sol-gel solution) by this method [27,80].

Appasamy et al. used spin coating and sol-gel synthesis to produce N-doped TiO_2 on SWCNT to develop a self-cleaning coating for photovoltaic systems [77]. For the synthesis of TiO_2 , TTIP and TOBT were dissolved in ethanol and a solution of ethanol, nitric acid and ammonia solution was added. After the reaction, the material was first dried and then calcined at 400 °C to obtain a powder. This powder was then added to a solution of

isopropanol and SWCNT using ethanol and, after the addition of acetic acid, reacted for several hours at 80 °C before the mixture was dried again. Spin coating was used to deposit the obtained powder in DMF onto glass samples. Nitrogen doping facilitated the formation of anatase and prevented the formation of brookite.

To prepare a composite material of N-F-TiO₂ and reduced graphene oxide (rGO), Jiang et al. used a sol-gel route [79]. For this purpose, they dissolved TOBT with ethanol and mixed it. A further solution of ethanol, water, acetic acid, carbamide, sodium fluoride, and rGO was prepared and added to the former one. After a gel was formed after one day, glass was coated using a vacuum rotary coating apparatus. The coated substrate was annealed at 400 °C for two hours to obtain anatase modification.

Besides dip coating and spin coating, impregnation is a third method that can be applied with a sol-gel suspension. It is to be noted, that published synthesis protocols do not always strictly distinguish between dip coating, immersion, direct coating, and/or impregnation. Usually, during impregnation, a substrate is immersed into a solution or suspension containing the coating material and stored there for a certain time [56]. This way, glass fiber tissues could be impregnated in a suspension of P25 [26,103].

Ho et al. coated La-doped titania onto ceramic filters by both dip coating and impregnation [46]. For that, they used a sol-gel route with TOBT as precursor and a lanthanum source. Doping with La prevented the modification change from anatase to rutile.

Zadi et al. mixed nanoparticles, namely silica and titania (PC500), with water in a ratio of 40/60% and coated the suspension on glass fibre tissues by using a press [104].

Thuy et al. impregnated titania nanotubes for air purification with different metals [88]. For this purpose, P25 was dispersed in sodium hydroxide solution for 20 min. This was followed by hydrothermal treatment at 135 °C for 24 h in an autoclave. After filtration and dispersion in nitric acid, the product was separated and purified with water. It was then dried and annealed at 500 °C. The synthesis was based on a protocol published by Nguyen et al. [105]. Before annealing, the basis for modification was established via impregnation with various metal salts, namely Zn(NO₃)₂, Cd(NO₃)₂, Al(NO₃)₃, Cu(NO₃)₂ and Fe(NO₃)₃. Impregnation of fibreglass was then carried out with the photocatalyst dispersed in water.

Two different photocatalysts, namely Ag@TiO₂-Cu²⁺@perlite and TiO₂-Cu²⁺@perlite, were prepared by Martínez-Montelongo et al. [65]. A sol-gel synthesis served as the basis. For the photocatalyst, copper sulfate in glacial acetic acid was mixed with TTIP. Separately, an aqueous solution of arabic gum was prepared and then added to the former solution. After drying and calcination at 300 °C, the particles could be further processed. The sol was applied to the perlite by impregnation. Two ways were mentioned for the incorporation of silver. First, silver was applied directly to the prepared TiO₂-Cu²⁺ powder via reduction of silver nitrate with NaBH₄ in a solution of sodium citrate and ethylene glycol, and second, silver was deposited on TiO₂-Cu²⁺@perlite via reduction. The obtained photocatalyst had anatase modification.

3.2. Spray and Electrospray Coating

In spray coating, the synthetic material is coated onto a surface by using a nozzle. This process is particularly suitable for large surfaces [16,106,107]. Parameters such as mechanical properties and morphology depend on various factors such as particle size, nanoparticle concentration, and the substrate [56]. A much rougher surface can be obtained by spray coating compared to dip and spin coating or impregnation [23,95]. This helps to increase the surface area of the heterogeneous catalyst and its photocatalytic activity [95]. Very similar to dip coating, spray coating uses suspensions of nanoparticles that are to be sprayed with a solvent (e.g., water) or a binder (sol, silane coupling agent) [90,95,106,108,109]. Sometimes, electrospray coating is applied. Here, the sprayed liquid or suspension is first charged by electrical forces at a high voltage. Subsequently, the charged droplets are sprayed from the tip of the nozzle to the substrate that needs to be coated.

Yu et al. electrosprayed P25 onto stainless steel surfaces pre-coated with SiO₂ for applications in the field of water purification [89].

Lettieri et al. coated stone samples by a spray coating procedure. To prepare the photocatalytic material, a hydrothermal method according to Pal et al. was applied [110–112]. For this, TTIP was added to acidified water. After two hours of reaction at temperatures just below 80 °C, the intermediate product obtained was treated in an autoclave for 30 min at 135 °C, resulting in crystalline nanoparticles. The coating was carried out by using an aqueous sol with the produced nanoparticles.

Nitrogen-doped nanoparticles were prepared by Chen et al. For this purpose, TOBT was mixed with water and ethanol at about 85 °C, dried at 80 °C and annealed at 400 °C. The powder obtained was mixed with urea, crushed and annealed at up to 500 °C for several hours. The obtained doped product was mixed with a silane coupler and the solution was spray coated onto asphalt [90].

The titanium dioxide sol can be also spray coated directly [23]. The corresponding sol was prepared via TTIP in ethanol. Zirconium tetrabutoxide was added to the solution. After stirring, a mixture of deionized water and perchloric acid was added. To spray the obtained sol onto glass, a binder solution of tetraethyl orthosilicate, colloidal silica, hydrochloric acid and isopropanol was prepared and mixed with the previously synthesized sol, propanol, and 2-propoxyethanol. An antase modification was formed.

Mahy et al. used silver-doped P25, which they spray coated after synthesis [109]. For the synthesis, first TTIP was mixed in methanol, P25 was added and the dispersion was heated. Silver acetate was then dissolved in 2-methoxyethanol and shaken. After half an hour, N-[3-(trimethoxysilyl)propyl]ethylenediamine was added and after 30 min, water with methanol, and finally P25 suspension were added. The solution was spray coated onto stainless steel [91,109]. In addition, the group was able to show that the temperature and the calcination time influence the formation of the crystal structure and modification. At lower temperatures, a longer duration is necessary to form a crystalline structure. If the temperature is too low, no phase transformation takes place even after a longer period of time. In addition, silica prevents the transformation from amorphous structure to anatase. Doping with silver leads to decreasing crystallinity.

3.3. Alternative Synthesis and Deposition Methods

There are several other ways to coat titanium dioxide onto a substrate. One of these possibilities is the anodization of titanium metal and creation of a titanium mesh sheet modified with titania nanoparticles (TMiP), as shown in Figure 9 by Ochiai et al. [113]. First, a titanium sheet was coated on both sides with resistant patterns and then titanium was dissolved on the uncoated areas via an acid bath. In a phosphoric acid bath, the resulting Ti-mesh was exposed to a voltage of 70 V and heated to 550 °C for several hours, resulting in TiO₂ on the surface. In addition, the obtained part was dipped into a sol of titania and then heated to 550 °C to make the particles adhere to the surface. A combined morphology of anatase and rutile (16%) was obtained.

Saran et al. synthesized (rutile) Ag-doped TiO₂ with TTIP in ethanol [114]. They added silver nitrate and, after 30 min, nitric acid. The sol was directly deposited on Pyrex glasses and calcined at 500 °C after drying.

Gryparis et al. synthesized a carbon-modified titanium dioxide for use in cementitious mortars [42]. For the preparation of the carbon dots, they dissolved citric acid and hydroxylamine hydrochloride in water and heated the mixture to 300 °C. The mixture was then used for the production of the titanium dioxide. After a few minutes, they dissolved the obtained solid in water, deagglomerated the particles and filtered the solution. For the synthesis of titanium dioxide, water and ethanol were added to the remaining clear solution. Subsequently, TTIP in ethanol and hydrochloric acid was added. After several hours of reaction at 80 °C, the solid was centrifuged, dried, and annealed at 200 °C for 2 h. In an FX-C consolidant, the obtained particles were brush coated. It was shown that in the synthesis of the undoped titanium dioxide, the pH value influenced the modification. A pH of 1.5 led to anatase and brookite, while at 2.5 only anatase could be detected. The modification with carbon resulted in an anatase structure.

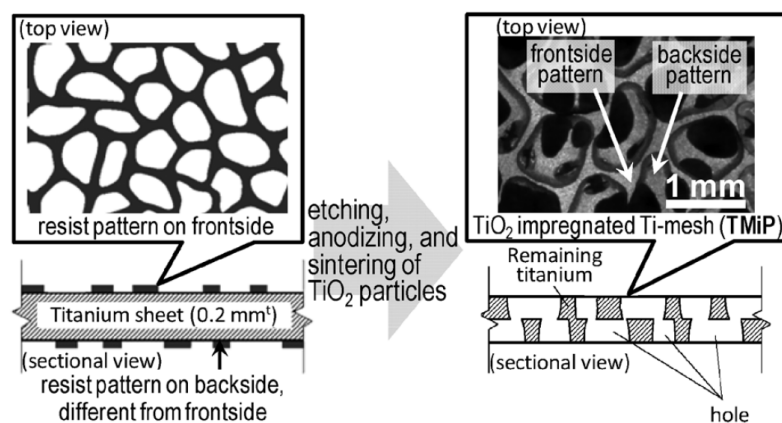


Figure 9. Production of a titania nanoparticles impregnated mesh filter via etching, anodization, dip coating, and sintering. (Reprinted/adapted with permission from Ref. [113]).

Colangiuli et al. mixed titania nanoparticles with a fluoropolymer precursor and water and brushed it onto a limestone surface. An anatase modification was present for undoped titania. For doped titania, a rutile diffraction pattern was observed with XRD.

Saran et al. prepared a silver-impregnated TiO_2 via TiO_2 powder in water [115]. To this, they added a silver nitrate solution, reduced it over dissolved SnCl_2 to elemental silver before heating the powder at $400\text{ }^\circ\text{C}$. A nanoparticle dispersion (anatase) in a slurry was finally used for brush coating onto ceramic three times and dried under sunlight conditions.

For their antimicrobial coating, Krishna et al. suspended anatase in NaOH solution [116]. A solution of polyhydroxy fullerenes was added and the obtained suspension was deposited on multiple substrates.

Another common method to produce metal oxide films such as titanium dioxide films is chemical vapour deposition (CVD). In this process, a substrate is placed in vacuum, while it is exposed to a reactant gas atmosphere containing precursors for the formation of a solid titania film (anatase) on the substrate [56,81].

Villard de Oliveira et al. used this method to deposit a Ti-Cu-O layer on single-crystal silicon and borosilicate (Corning C1737) [82]. Titanium(IV)oxide bisacetylacetonate in ethanol with Cu(II)acetylacetonate in ethanol with ethylene diamine was used as precursor. A mixed modification of anatase and rutile (17%) was achieved.

Krumdieck et al. used pp-MOCVD (pulsed pressure metal-organic CVD) to coat stainless door handles with titania [81]. TTIP in toluene served as the reactant.

Saqlain et al. applied temperature-regulated CVD to coat TiO_2 with Fe [63]. P25 served as substrate and biscyclopentadienyl iron as iron source. The CVD was carried out in water vapor in oxygen-air atmosphere, while the ferrocene was vaporized at $60\text{ }^\circ\text{C}$. After its deposition, the ferrocene was oxidized at $200\text{ }^\circ\text{C}$. The sample was then calcined at $750\text{ }^\circ\text{C}$ for 8 h. The obtained particles were poured onto stainless steel in dispersion of isopropanol. The high calcination temperature converted the anatase-rutile mixture to rutile.

In addition to CVD, physical vapour deposition (PVD) or sputtering have been reported as deposition methods for titania films. In general, in PVD a solid phase (target; electrode 1) is transferred into the gas phase and a film is created on the surface of a substrate (electrode 2) by subsequent condensation. In sputtering, atoms are released from the surface via high-energy bombardment, mostly with cations. These ions are then deposited on the surface again [34,56].

Milićević et al. coated glass samples and silicon wafers with titanium dioxide and gold by using PVD [47]. The corresponding metals served as gold and titanium source. The deposition was carried out in an oxygen atmosphere. First, titanium dioxide, then gold and finally titanium dioxide was deposited on the surface. The coated samples were annealed at $400\text{ }^\circ\text{C}$ for several hours in a nitrogen atmosphere to obtain anatase modification.

In addition, the magnetron sputtering PVD technique by Rupp et al. was used to coat silicon wafer stripes and capillary tubes with TiO₂ (anatase) [117].

Photocatalysts can also be incorporated into a paint and then applied to, e.g., a wall or ceiling. Maggos et al. synthesized a photocatalyst called TCM-1 by preparing a solution based on titanium(IV) oxysulfate hydrate, manganese and ammonia [92]. After ageing the mixture overnight, a powder was obtained via filtration and drying. This was crushed and annealed at 700 °C for several hours. The product was then incorporated into a wall paint consisting of typical wall paint ingredients. A similar principle was used by Maurer et al., whose air purifier was based on the photocatalytic paint PureTi™ [25].

The photocatalyst can be also embedded directly into the substrate or the substrate already consists (partially) of the photocatalyst. Dalanta et al. prepared a membrane by using this approach [83]. For this, SiO₂ was first dissolved in sodium hydroxide solution and undissolved particles were separated. Titania and CoCl₂ were added subsequently. The dispersion, was acidified with hydrochloric acid, and after reaction, the obtained gel was dried, annealed at 500 °C, and crushed into particles. The membrane was produced via induced phase separation. First, polysulfone was dissolved in NMP and then the nanoparticles were added. After stirring for 12 h and simultaneous dispersion, the solution was poured onto a glass plate and stored in water for 24 h. This produced a membrane film (anatase modification), which was finally dried.

Horváth et al. prepared a water filter, which consisted partially of titania nanowires [84]. The nanowires were produced by heating titanate (H₂Ti₃O₇). Furthermore, carbon nanotubes (CNT) were produced for the filter via CVD. The two components were mixed and applied via doctor blading. [84] Doctor blading describes a process in which a solid-liquid mixture is applied to a substrate and then spread with a doctor blade, to form a film [56]. The obtained films were dried and annealed at 600 °C, which converted titanate into anatase and also achieved a mechanically more stable network.

In Table 1 (undoped) and Table 2 (doped and modified) multiple photocatalysts, their synthesis route, the applied deposition method, and their anticipated field of application are summarized.

Table 1. Synthesis methods, obtained titania modifications (if known), deposition technique, and anticipated application for undoped TiO₂ photocatalysts.

Photocatalyst	Titania Synthesis Route	Modification	Deposition Method	Substrate	Later Application	References
TiO ₂	Italcementi, TX-Active [®] and TX-Boosted [®]	-	spray coating	wall	air purification	[16,106,107]
TiO ₂	titanium and sol	anatase and rutile (minimal amount)	anodization and dip coating	titanium	air purification	[24,113,118]
TiO ₂	PureTi TM	-	-	fiber-reinforced plastic	air purification	[25]
TiO ₂	P25	anatase (80%) and rutile (20%)	impregnation	glass fiber tissue	air purification	[26,103]
TiO ₂	-	anatase	spin coating	glass	antimicrofouling	[80]
TiO ₂	precursor	anatase and rutile (17%)	CVD	stainless steel	antimicrobial	[81]
TiO ₂	heating titanate	anatase	doctor blading	matrix with carbon nanotubes	water purification	[84]
TiO ₂	sol-gel	anatase and rutile (16%)	dip-pad	ceramized fabrics	water purification	[87]
TiO ₂	P25	(anatase)	spray coating	SiO ₂ @stainless steel	water purification	[89]
TiO ₂	P25 and PC500	anatase and rutile (<20%)	dip coating	Cellulose acetate monolithic	air purification	[93]
TiO ₂	-	-	spray coating	fiberglass	air purification	[95]
TiO ₂	P25	anatase (80%) and rutile (20%)	dip coating	porous alumina membrane	water purification	[96]
TiO ₂	sol-gel	anatase	dip coating	cellulose acetate monolith	air purification	[97]
TiO ₂	sol-gel	anatase	dip coating	glass	water purification	[99]
TiO ₂	sol-gel	anatase	dip coating	porous ceramic foam filters	air purification	[102]
TiO ₂	PC500	(anatase)	impregnation	glass fiber tissues	air purification	[104]
TiO ₂	-	-	spray coating	bituminous pavement	air purification	[108]
TiO ₂	sol-gel	-	spray coating	limestone	self-cleaning	[111]
TiO ₂	-	-	brush	limestone	self-cleaning	[119]
TiO ₂	-	anatase	PVD	silicon wafer stripes and capillary tubes	medical application	[117]
TiO ₂	TiO ₂ -suspension	-	immersion	cellular ceramics	water purification	[120]
TiO ₂	PureTi TM	-	spray coating	fiber-reinforced plastic	air purification	[121]
TiO ₂	TiO ₂ containing paint	-	-	wall	air purification	[122]

Table 2. Synthesis methods, obtained titania modifications (if known), deposition technique, and anticipated application for doped or modified TiO₂ photocatalysts.

Photocatalyst	Titania Synthesis Route	Modification	Deposition Method	Substrate	Later Application	References
Zr-TiO ₂	sol-gel	anatase	spray coating	glass	self-cleaning and antifogging window glass	[23]
Ag-TiO ₂	sol-gel with P25	anatase	spray coating	stainless steel	water purification	[91,109]
Mn-TiO ₂	precursor	anatase	dispersion	wall	air purification	[92]
N-TiO ₂	sol-gel	-	spray coating	asphalt	air purification	[90]
C-TiO ₂	sol-gel	anatase	brushed	cementeous mortar	self-cleaning	[42]
La-TiO ₂	sol-gel	anatase and rutile (minimal amount)	impregnation	porous ceramic air filter	air purification	[46]
Au-TiO ₂	titanium	anatase	PVD	silicon wafers and microscopic glass	-	[47]
Ag-TiO ₂	P25	-	dip coating	glass fiber	air purification	[62]
Fe-TiO ₂	P25	rutile	pouring	stainless steel	air purification	[63]
Ag-TiO ₂ -Cu ²⁺	sol-gel	anatase	impregnation	perlite	air purification	[65]
N-TiO ₂ /SWCNT	sol-gel	anatase	spin coating	glass	self-cleaning	[77]
N-F-TiO ₂	sol-gel	anatase	vacuum rotary coating	glass sheet	building glass	[79]
Ti-Cu-O	precursor	anatase	CVD	single crystal and boroaluminosilicate	antibiofouling	[82]
Co-TiO ₂	sol-gel	anatase	induced phase separation	matrix with SiO ₂	water purification	[83]
Bi-TiO ₂	sol-gel with P25	-	immersion	glass spheres	water purification	[86]
Al/Zn/Cd/Cu/Fe-TiO ₂	P25	-	impregnation	fiber glass	air purification	[88]
Cu-Ag-TiO ₂	P25	anatase	dip coating	optical fiber	air purification	[94]
N-TiO ₂	sol-gel	anatase	immersion	ultrafiltration membrane	water purification	[98]
Ag-TiO ₂	sol-gel	rutile	-	Pyrex glass	water purification	[114]
Ag-TiO ₂	P25	anatase	brush coating	ceramic	water purification	[115]
TiO ₂ /polyhydroxy fullerenes	-	anatase	-	surface	antimicrobial	[116]
C-TiO ₂	-	anatase	spray	bituminous asphalt	air purification	[123]

4. Applications

The vast majority of already realized applications—or at least of applications in a prototype stage—of photocatalytically active titania composites cover the fields of air purification, self-cleaning and antimicrobial surfaces, and water purification. A few selected example applications that are well described in publicly accessible databases are presented in this section. We made our selection also dependent on the existence of reliable measures to really prove and ideally quantify the photocatalytic effect of the prepared materials and systems. In addition, general studies evaluating the photocatalytic effect in realistic scenarios will be discussed as well.

4.1. Photocatalytic Air Purification

Saqlain et al. built a prototype reactor for the purification of pollutant-enriched gases with iron-modified titanium dioxide [63]. The group prepared the photocatalyst via CVD from P25, while varying the iron content (0.1, 0.6, 1.8 wt%). The photocatalytic property was characterized by the degradation of acetaldehyde in the prototype reactor. The photocatalyst was casted in isopropanol on stainless steel. The catalyst was irradiated with visible light in the reactor. It could be shown that Fe-TiO₂ with 0.1 wt% iron degraded 65% of the initial acetaldehyde concentration. The degradation efficiency decreased with increasing iron content. The degradation in the reference measurement with pristine calcined TiO₂ was between that of iron with 0.6 and 1.8 wt%.

Monteiro et al. invented a compound parabolic collector (CPC) single-pass reactor on a pilot scale for removal of *n*-decane in indoor air. The aim was to develop a continuous purifier for 24 h a day with artificial UV radiation and solar light. Two types of titanium dioxide were used as photocatalyst, namely P25 and PC500, which were applied to monolithic cellulose acetate via dip coating from an aqueous solution. The reactor consisted of multiple 1.5 m long pyrex glass tubes (70 mm diameter) with a further, inner quartz glass tube. The photocatalyst was placed between outer and inner glass tube. The UV source was located in the inside of the inner tube. The setup was placed on the CPC. The reactor was fed with *n*-decane (10 ppm) with a flowrate of 2 l min⁻¹. Monteiro et al. observed that different light intensities and a mixture of solar and UV radiation were necessary at different times (i.e., morning and afternoon). This was assigned to the dependence on adsorption-desorption processes and temperature. Overall, *n*-decane removal for P25 and PC500 was up to 71% and 100%, respectively [93]. In a subsequent project based on these findings, titania films were synthesized by a sol-gel method with the aim to prepare a translucent anatase film for increased transmittance of UV radiation [97]. The reactor was the same as explained by Monteiro et al. [93]. As result, under outdoor conditions, *n*-decane could be removed completely.

Ho developed a ceramic foam air filter coated with mesoporous TiO₂ for photodegradation of NO [102]. His aim was to substitute conventional TiO₂ thin films by mesoporous films with higher surface area with more active sites. He coated the aforementioned filter with a reverse micellar method. For characterization of the photocatalytic activity, Ho measured the degradation of NO (1000 ppb or 400 ppb) in a continuous flow reactor (4 l min⁻¹). Moreover, TiO₂-coated tiles were compared to previously described mesoporous structures. Ho observed 92.5% degradation of NO in a single pass. Additionally, the porous structure had two special advantages in comparison to planar TiO₂ films: a higher surface area led to higher photocatalytic activity and a porous structure caused turbulences and mixing of air stream which, in consequence, supported contact between pollution and catalyst. Even after multiple cycles, no deactivation of the catalyst could be observed.

Thunyasiriron et al. studied the substitution of expensive HEPA filters by cheaper air filters based on (metal-doped) TiO₂ coated glass fibers [62]. They coated two different-graded glass fibers with 5% TiO₂. Either polyethylene glycol, silane or DURAMAX™ in multiple concentrations were used as binders for coating support. In addition, the doping with silver and iron was investigated to increase the photocatalytic activity. Moreover, some additionally influence factors such as air velocity of a model air purifier and relative

humidity were evaluated. Degradation of *Mycobacterium tuberculosis* served as indicator for photocatalytic activity. Overall, it was observed that 3% of DURAMAX™ as binder exhibited the highest photocatalytic activity. In addition, 0.1% metal doping with either iron or silver caused a 100% degradation. Silver led to higher degradation efficiency due to its antimicrobial effect. Conducted experiments indicated a negative effect of high humidity and increased flow rate.

Zadi et al. studied the abatement of trichlormethane in hospital rooms by using a novel air purification system [104]. The group constructed a prototype reactor utilizing both a non-thermal plasma and a photocatalyst. The reactor was cylindrically shaped and had an inner and outer pyrex tube. In the inner tube, a UV lamp was installed. In between the tubes, a glass fiber tissue consisting of—among other materials—impregnated titania. The gaseous effluents could flow through this glass fiber tissue. The outer tube was covered by a rolled-up copper electrode. As inner electrode, two rolled-up rails of metal spread were installed. The reactor was used to investigate the effect of gas flow rate and relative humidity. Zadi et al. concluded, that combination of both systems (i.e., non-thermal plasma and a photocatalyst) increased the degradation in reference to only one system or just combining both systems. Additionally, the increased flow rate ends up in less degradation, while an increased humidity causes an enhanced degradation due to the improved formation of hydroxyl radicals.

The photocatalytic activity of La-doped titania coated onto a commercial ceramic filter by Ho et al. was studied by the degradation of both NO and acetone in dependence on humidity [46]. For acetone, the photocatalytic degradation decreased beyond 10% relative humidity due to condensation of water and subsequent blocking of active surface states. At 100% relative humidity, an increasing activity was observed due to formation of more radicals, i.e., hydroxyl radicals and hyperoxide anion radicals. For NO, the influence of humidity was slightly different. Here, 20 to 60% relative humidity exhibited the highest degradation efficiency. Photocatalytic removal of NO (98%) and acetone (38%) was higher for La-doped TiO₂ than for pristine titania (NO: 65%; acetone: 28%) under visible light. Ho et al. also pointed out the advantages of the porous structure, i.e., more adsorption sites and reactive surface states.

Abou Saoud et al. investigated a pilot reactor with a new reactor material and design [94]. Optical fibers, made of both polymer fibers and polyester fibers and part of it with an additional metallic wire (Ag or Cu), were woven. Those fibers were dipped in an aqueous suspension of P25 with the aim of immobilizing titania nanoparticles on the surface. In consequence, there were three types of support on fibers: TiO₂, TiO₂-Ag, and TiO₂-Cu. The woven textile was put into a glass chamber with UV lamp. Air flow consisting of either butane-2,3-dione/heptane-2-one as VOC, *Escherichia coli* as bacteria, or combination of one of the VOC and the bacteria was directed through the woven textile. In addition, they varied multiple factors, i.e., initial concentration of pollutant, flow rate, and relative humidity. It was shown that an increasing flow rate led to a decreased degradation efficiency of butane-2,3-dione. An increased humidity ended up in a decreased degradation/inactivation of both butane-2,3-dione and *E. coli*, and a higher initial concentration of pollutant caused a decreased degradation of butane-2,3-dione. Pure titania fibers had approximately no bacterial inactivation effect, but showed 63% of butane-2,3-dione degradation. TiO₂ exhibited lower degradation of butane-2,3-dione than TiO₂-Ag, followed by TiO₂-Cu. Values of the VOC removal efficiency were 47% and 52% for TiO₂-Ag and TiO₂-Cu, respectively. Moreover, combined pollution of VOC/bacteria resulted in higher degradation/inactivation than just observed for a single pollutant.

Schnabel et al. developed a novel flow-through titania photocatalytic system [95]. Their aim was to evaluate different experimental settings and boundary conditions under UV radiation. A titania coated fiberglass served as photocatalyst. Titania was applied by spray coating which led to a rough surface with a high surface area. The complete device had a size of 120 × 11 × 60 cm³, consisted of fans (up to 50 m³ h⁻¹), photocatalyst and UV lamp (Figure 10). The reactor system was tested under laboratory conditions

with naphthalene and 1-methylnaphthalene as pollutant. Later on, the device was tested in two office rooms with high and low pollutant concentrations, respectively. The first room was not in use during experiment, the second one was used normally. Under laboratory conditions, a fast and complete removal of pollutants was observed. No further byproducts were detected. Under real conditions, in room 1 and room 2 degradation of naphthalene and other chemically similar pollutants achieved a reduction by up to 66% and 80% respectively. It could be proven that the degradation rate is sufficient to reduce a harmful concentration of pollutants in real environments in a fast way.

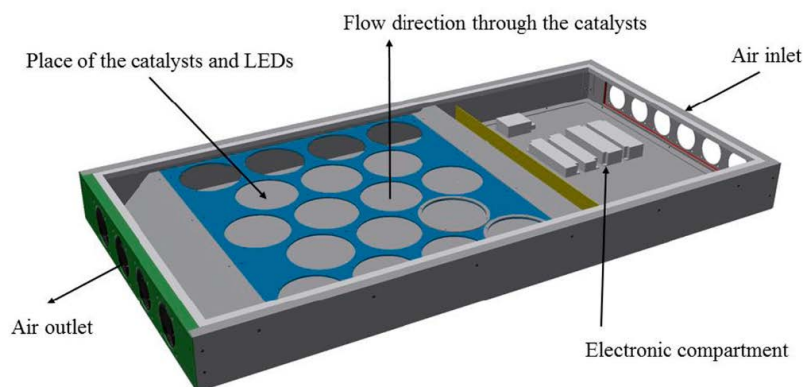


Figure 10. Model of an air purifier built by Schnabel et al. (Reprinted/adapted with permission from Ref. [95]).

Thuy et al. measured the air pollution in field tests while burning incense materials [88]. They investigated air purifiers based on Cd, Zn, Al, Cu, or Fe-doped titania nanotubes impregnated on fiberglass. The fiber glass was put into a box with air inlet on the one side and outlet on the other side. Additionally, an UV lamp was placed inside the box. For air purification measurements, they burned an incense with previously detected highest VOC pollution. It was found that Zn-TiO₂ showed the highest VOC removal from 5409 ppb to 2391 ppb within 5 min (Figure 11). After further 30 min, this value decreased to 249 ppb. All further photocatalytic probes reached this value after more than 50 min. The specific effect of Zn might, however, also be caused by a higher surface area of this particular photocatalyst. Interestingly, all other tested metal-doped TNTs had a smaller efficiency as compared to neat TNT.

Three different types of air quality control equipment, namely full-covering type, underneath swinging type, and lateral swinging type, were installed in a Taiwan medical nursing institution [124]. Every air quality system was complemented by a silver doped titanium dioxide photocatalyst, UV lamp, and fan. The exact synthetic route was not given for confidentiality reasons. While the measurement took place for 24 h, the restrained bacterial rate was documented. 90 cm above ground, it was observed that full-covering type, underneath swinging type, and lateral swinging type had a restrained bacterial efficiency of 71, 50, and 45%, respectively. The full-covering air quality control was also used for air purification in a museum. There, the restrained bacterial efficiency was even higher with up to 92% after 24 h. Additionally, Sung et al. concluded that higher initial concentrations led to higher disinfection efficiency. The higher degradation in the museum than in the nursing institution was assigned to the different resistances of the respective bacterial strains [125].

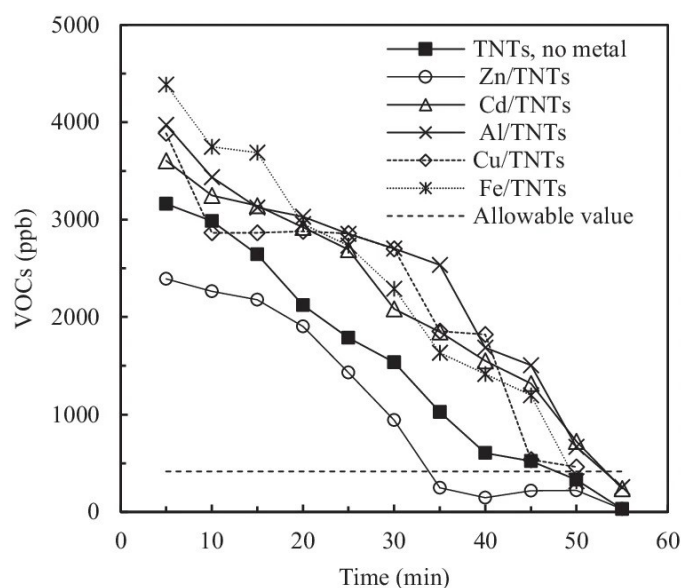


Figure 11. VOC degradation of different metal-doped titania nanotubes. (Reprinted/adapted with permission from Ref. [88]).

Ochiai et al. investigated an air purifier consisting of both photocatalyst and plasma [24]. Both techniques, namely TMiP for photocatalysis and PACT for plasma purification, were described in a separate publication in detail [113]. In TMiP a titania mesh filter was synthesized via etching and anodization, and dip coated with TiO_2 nanoparticles. With this approach, air was purified from both VOC and total suspended particles (TSP) in a smoking room. For this purpose, a prototype (Figure 12) consisting of HEPA filter, PACT-TMiP, ozone cut filter, activated carbon filter, and fan was installed in a smoking room in an originally non-smoking office. After burning eight cigarettes and consequently increasing concentration of pollutants, it could be shown that most products were removed or degraded. Figure 13 illustrates the degradation of ammonia, acetaldehydes, and acetic acid with the combined and individual purification steps. The combination of all methods always had the strongest air-purifying effect, even if the individual purification methods did not have great efficiency. Moreover, this air purifier was tested in long term use. Even after 21900 smoked cigarettes the removal efficiency of TSP remained higher than 98.5%. The removal efficiency of VOC decreased after 12000 and 21900 smoked cigarettes to 88% and 43%, respectively.

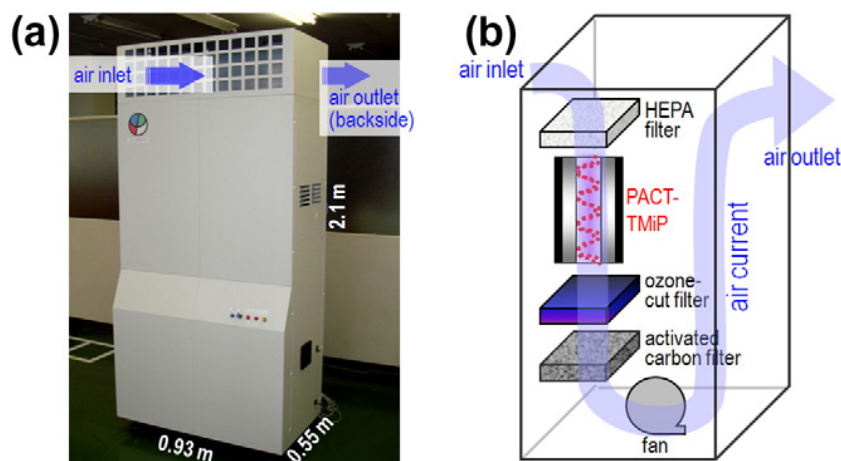


Figure 12. Device (a) and schematic construction (b) of an air purifier for cleaning air in smoking rooms. (Reprinted/adapted with permission from Ref. [118]).

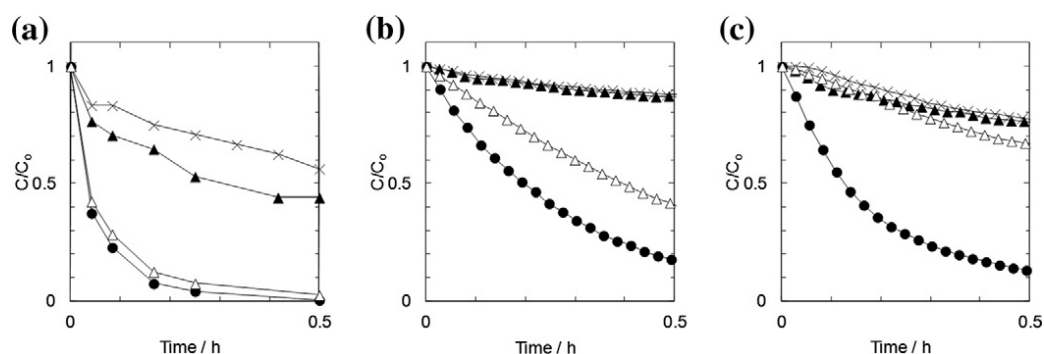


Figure 13. Degradation of ammonia (a), acetaldehyde (b), and acetic acid (c) with the combined air filter (filled circles), only PACT (empty triangles), only the TMiP filter (filled triangles) and without filter (crosses). (Reprinted/adapted with permission from Ref. [118]).

Assadi et al. tried to reduce pollution in exhaust gases from animal quartering home centers by a pilot scale and an industrial scale air purifier [26]. For that, degradation of ammonia and multiple VOC were measured. The reactor was built of both titania nanoparticle impregnated on glass fiber tissue and a surface discharge plasma [103]. A detailed overview of the reactor design is displayed in Figure 14. At the laboratory scale, the removal efficiency of isovaleraldehyde for only plasma and only photocatalysis was approximately 20% and 38%, respectively. The combined process had a removal efficiency of up to approximately 66%. On industrial scale, photocatalytic degradation of the aforementioned pollutants and two further aldehydes was between 21 and 24%, and ammonia degradation was 25%. Degradation of multiple aldehydes (except isovaleraldehyde) by only plasma was up to 35%. Degradation efficiency of isovaleraldehyde was approximately 10%. Combination of plasma and photocatalysis led to a removal efficiency for aldehydes of between 60 and 75%. Regarding to non-stable conditions, in industrial scale the higher efficiency of the combination of plasma and photocatalysis could not surely be proven. Especially at pilot scale, CO_2 was the main product of pollutant degradation due to complete oxidation of by-products formed by plasma reaction.

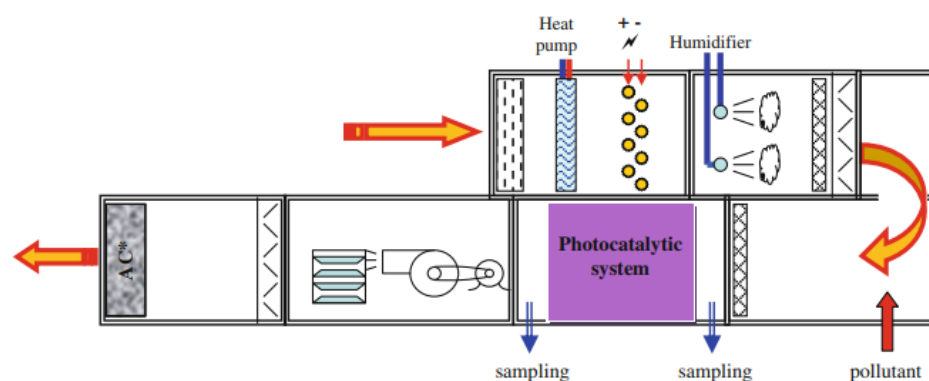


Figure 14. Design of an industrial-scale air purifier for the purification of exhaust gases from an animal shelter. (Reprinted/adapted with permission from Ref. [26]).

Maurer and Koziel studied the removal of VOC, odor, ammonia, H_2S , and greenhouse gases by a titania paint (PureTi™) based air purifier system in exhaust gases of a swine barn for two months [25]. The flow-through reactor was built of titania painted wall panels, an UV lamp, and a fan for ventilation. They observed a decrease of p-cresol (22%), odor (16%), and N_2O (9%), while CO_2 was increasing by 3% due to photocatalytic degradation of organics. No removal of multiple further VOC was observed.

PureTi™-based air purifier technology was also used by Lee et al. [121]. Odors, VOCs, ozone, nitrous oxide, and ammonia were successfully removed, while H_2S , methane gas, and CO_2 remained in the exhaust gas.

Another prototype air purifier was developed by Martínez-Montelongo et al. using photocatalytic material based on $\text{TiO}_2\text{-Cu}^{2+}$ /perlite and $\text{Ag@TiO}_2\text{-Cu}^{2+}$ /perlite [65]. For this purpose, they placed the coated perlite in a glass cylinder, 50 cm long and 2.5 cm in diameter, and fed air samples from several dental clinics under UV-VIS light irradiation in separate experiments. They examined the quality and quantity of bacteria in the air. Among others, *E.coli*, *S. aureus*, *Y. enterocolitica*, *Enterobacter aerogenes*, *Serratia* sp., *Bacillus* sp., and *Staphylococcus epidermis* were found. The authors used a Thermo Scientific™ Six Stage Viable Andersen Cascade Impactor to separate the samples according to particle size (level 1–2: non-respirable bacteria; level 3–6: respirable bacteria) and finally analyzed them bioanalytically. Compared to the reference measurement without air filter, the preliminary and main experiments always showed a significantly lower load of colony forming units as far as the air filter was used (Figure 15). The authors concluded that the efficient air purification basically depends on purity, composition, specific surface area, and crystallinity of the used photocatalyst. They also stressed the importance of enhanced surface electronic effects.

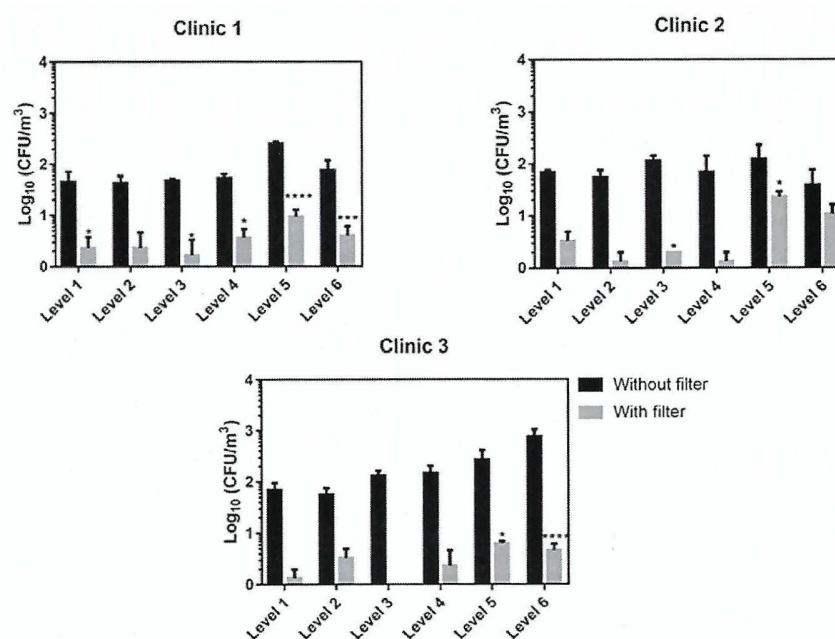


Figure 15. Differently sized bacteria (Level 1: huge (non-respirable); Level 6: small (respirable)) in three different dentistry clinics with and without air purifier. The stars refer to Sidak's multiple comparisons test with *: $p < 0.01$; **: $p < 0.002$; ***: $p < 0.0001$. (Reprinted/adapted with permission from Ref. [65]).

Blondeau et al. tested six commercially available air purifiers using different cleaning techniques [126]. Their aim was the evaluation of both pollutant removal efficiency and computed energy efficiency. The tested devices used mechanical filtration, electrostatic precipitation, gas filtration, ionization, cold plasma, and photocatalytic oxidation. The purifying efficiency was tested with particles, a mixture of multiple VOC, and two bacteria strains. As a result, photocatalytic oxidation had no significant influence on degradation of VOC and bacteria, while its energy consumption was high compared to particle filter/activated carbon filter and electrostatic precipitator.

Ehm et al. investigated the photocatalytic NO_x depollution by actively vented air purifiers in a highway tunnel in Berlin, Germany [127]. In their study, a special focus was put on the CFD simulation of the surface geometry of photocatalyst, the internal design of the reactor, the tunnel's internal air flow and concentration profile, and on the placement of the reactor inside the tunnel. Based on their simulation, a reactor was built and tested for real NO_x depollution in the tunnel. A reactor consisting of both TiO_2 -dispersion coated foam radiated with UV light and active ventilation led to 25% removal of NO_x . They concluded that the optimal air purifier necessitates a high reaction surface geometry

combined with a high volume flow. Furthermore, the air purifier has to fit to the tunnel's geometry. Most pollutants should hit the active sites of the photocatalyst and nearly the complete tunnel air has to reach the reactor before leaving the tunnel.

Air disinfection in a hospital room was investigated by using a Puradigm[®] air purifier. Garaibeh et al. wanted to use it to study the purification of the air from *Staphylococcus aureus* and *Clostridioides difficile*. In addition, air purification in a biosafety cabinet was explored with the dengue type 2 virus. Appropriate samples were placed in two identical hospital rooms (one for measurement, one as a reference) and degradation was measured in each room for 24 and 48 h, respectively. It was found that *Staphylococcus aureus* had the significantly higher concentration in the reference room (log CFU = 3.92) than in the measurement room with air purifier (log CFU = 1.35). For *Clostridioides difficile*, the values for log CFU were 2.8 and 0.7, respectively. Moreover, for the dengue type 2 virus, within 6 h, an 83.5% decrease in infectivity was observed with air purifier. The authors emphasized that such air purifiers work efficiently and can effectively reduce infectivity [128].

In the field of air purification, some photocatalytic systems are already commercially available. However, the used photocatalyst, mode of operation, purification efficiency, and energy consumption are most often not accessible in all details and hence cannot be evaluated here.

4.2. Self-Cleaning, Antifogging and Air/Water Purifying Building Materials and Coatings

Multiple building materials such as glass, stone, concrete, or asphalt, but also other materials such as optical glasses or medical instruments take advantage of the photocatalytic effect for self-cleaning, antifogging, antimicrobial or air purification applications. This chapter will present an overview of selected examples for these intriguing applications and of analytical setups to evaluate the photocatalytic effect.

The photocatalytic activity of titania coatings on building materials such as glass is often tested by the evaluation of dye degradation in aqueous solutions upon irradiation. Jiang et al. developed on a laboratory scale an N-F-TiO₂/rGO (TGNF) photocatalyst which was coated on glass [79]. The catalyst TGNF was prepared via a sol-gel route and deposited by a vacuum rotary coating apparatus. The group reports a methylene blue degradation of about 50% under UV-VIS irradiation after 2.5 h for this catalyst, whereas for N-TiO₂/rGO a value of 45% was obtained. The control samples, namely N-doped titania and pristine titania, exhibited a methylene blue dye degradation efficiency of approximately 10% and 6%, respectively. After seven replicate measurements, the degradation efficiency of TGNF decreased to only 40%, which is why the authors emphasize its stability and applicability in real systems.

Milićević et al. investigated a photocatalytically active Au-doped TiO₂ film, which was prepared by sputtering, by means of the degradation of Rhodamine B on a laboratory scale and compared it to pristine TiO₂. It was shown that the gold doped sample had a larger degradation effect under simulated solar light than pure TiO₂ [47].

For self-cleaning of glasses on photovoltaic systems, Appasamy et al. developed a composite material consisting of SWCNT and N-doped TiO₂ on glass [77]. The photocatalytic self-cleaning effect was tested by means of degradation of the dye methylene blue under visible light. It was found that the degradation of the dye was up to 72%, whereas the degradation with P25 was only about 50%. The degradation efficiency was very sensitive on the composition of N-TiO₂ and SWCNT. In some cases, even a degradation performance worse than P25 was obtained.

Dineshram et al. studied the antifouling effect of metal oxide based coatings on glass for marine optical instruments [80]. For that, multiple glass substrates were spin coated with aqueous dispersions of titania nanoparticles, niobia nanoparticles, or silica sol. Coated glass substrates were stored in real seawater for 15 days. After 4, 9, and 15 days, the number of oyster, hydroide, and barnacle on the surface was counted. It was observed that metal oxide coated glass mostly had higher fouling resistance than the control glass. After 9 days, macrofoulants steadily increased due to adsorbed foulants causing a barrier

between coating and foulant. The authors concluded that TiO_2 is the most promising candidate for minimizing biofouling on glass surfaces.

Gryparis et al. investigated a C-modified TiO_2 (called TC) for application on self-cleaning cementitious mortars [42]. At first, they studied the photocatalytic activity of different loaded (i.e., TC25 with 1.5 g and TC75 with 13.5 g C-Dots for 4.5 g TTIP) and tempered C-modified TiO_2 . They compared the performance with neat TiO_2 and Au- TiO_2 (TAu) by investigating the degradation of methyl orange under UV irradiation, simulated solar irradiation, and real solar irradiation. In addition, they dispersed the catalysts in a silica-based solution (FX-C) and brushed it onto cementitious specimen. The decolorization of methylene blue dye was measured on its surface. In Table 3 it is shown that with increasing C-dot concentration the photodegradation of methyl orange under UV light, artificial solar light, and visible light irradiation increased up to a certain point, while with very high concentrations the degradation efficiency decreased again. In addition, the dependence of the degradation efficiency on the used light source is also shown. Coated onto cementitious specimens, FX-C as well as double coated FX-C+(FX-C+TC25) offered the highest photocatalytic activity against pollutants. The degradation efficiency for methyl orange was lower after several cycles, but with longer reaction time, complete degradation was possible, so the authors characterized the catalyst as robust. The authors highlighted both the usability of C-dotted TiO_2 and the need of field tests.

Table 3. Methyl orange degradation efficiency per time for C-modified titanium dioxide (TC) in a binder for coating cementitious mortars under UV, visible, and sunlight irradiation. Different ratios of C-dots in contact with titania are presented (TC0: no C-dots; TC75: high loading). TAU means titania in contact with Au. (Reprinted/adapted with permission from Ref. [42]).

Irradiation	Photocatalyst	Degradation Rate (%)/min
UV-A light	TC0	45.5/60
UV-A light	TC25	96.2/60
UV-A light	TC50	90.9/60
UV-A light	TC62.5	62.9/60
UV-A light	TC75	46.1./60
Visible light	TC0	20.8/120
Visible light	TC25	91.4/120
Visible light	TC50	92.0/120
Visible light	TC62.5	56.9/120
Visible light	TC75	48.7/120
Solar light	TC0	48.1/60
Solar light	TC25	96.0/30
Solar light	TC50	90.2/30
Solar light	TC62.5	78.2/60
Solar light	TC75	71.0/60
Solar light	TAu	70.6/60

Maggos et al. investigated the photocatalytic reduction of NO_x gases in an artificial closed indoor car park [122]. For that, the ceiling was treated with TiO_2 -based paint. Then, car exhaust gas was injected into the car park and UV lamps were activated for 5 h. As a result, 19% of NO and 20% of NO_2 were removed. However, the authors reported lower NO_x removal than under laboratory conditions, possibly due to inhibitory effects from other pollutants.

Multiple studies of creating titania coated building materials such as tunnels, walls, and streets were accomplished within the EU-funded project PhotoPAQ (Demonstration of Photocatalytic remediation Process on Air Quality). In one sub-project, Gallus et al. built two identical artificial street canyons [16]. Walls were made of fiber cement boards. They split their project into two parts. In the first half, neither the reference nor the “active” street canyon was photocatalytically active. In the second half of the project, both walls and street surface of one of the street canyons were coated with a photocatalytically active mortar

(Italcementi, TX-Active™). All the time, multiple parameters such as concentration of NO_x, O₃, VOC, and airborne particles were measured. However, no significant degradation of NO_x pollution was found (limit of detection was 2%). Moreover, the removal of VOC could neither be proven. Additionally, the photocatalytically active material did not lead to a sufficient prevention of ozone formation. In the authors' opinion such results did neither fit to depollution tests in laboratory scale nor to former real site tests. They concluded that this is possibly due to transport limitations to the active sites, the geometry of the test spot, the sampling position, sampling period or differences between active and reference street canyon. Also they remark, that just this technique on its own is insufficient for solving the NO₂ pollution in European urban areas. Furthermore, the same photocatalytic paint and later on TX-Boosted™ was used to cover both ceiling and upper wall of the Leopold II tunnel in Brussels [106]. The aim was to track air depollution under artificial UV light. In consequence, no depolluting photocatalytic effect was observed. However, the authors mentioned some difficulties while performing the trial. It was concluded that the negative depollution effect might be due to the deactivation of the photocatalytic layer during installation of a more intensive UV light during an interruption interval of the experiment. In addition, high wind speeds resulted in short contact times of the pollutants on the catalyst and increased relative humidity led to blocked surface states. The deactivation was also assigned to blocked active surface states by carbon particles such as brake dust and adsorption of VOC. Because of such aforementioned reasons the authors recommended several points of improvement for further on-site studies. Gallus et al. made a model calculation based on laboratory and field test measurements for the aforementioned photocatalytic tests [107]. They concluded that with the given conditions, NO_x degradation should have been up to 0.4%, but this would have been lower than the experimental significance limit of 2%. Moreover, with optimal conditions and without passivation of samples, photocatalytic removal of NO_x can be increased up to 20%. Hence, they recommended careful characterization of tunnel conditions, quantification of the deactivation of photocatalytic material, modeling of estimated degradation rates and analysis of costs.

Chen et al. studied the photocatalytic effect and application's durability of N-doped titania immobilized on asphalt surfaces under UV and visible light irradiation [90]. They synthesized N-doped titania via a sol-gel route and sprayed it onto bituminous surfaces in both laboratory scale and real scale. Photocatalytic activity was evaluated on a laboratory scale (Figure 16). It was shown that N-doped TiO₂ had higher NO_x removal efficiency under especially visible light due to better light absorption and less energy required due to a smaller band gap. Moreover, the photocatalytic activity was dependent on the wavelength of the irradiation light. The removal efficiency for NO of doped TiO₂ were approximately 27.6% and 13.8% for 330–420 and 590–680 nm light wavelength range, respectively. Moreover, they observed a lower degradation for NO₂ than for NO, possibly due to the reaction mechanism. For durability tests, a real street was partially covered with N-doped TiO₂. While field tests were performed, the street was washed once per week. During the whole test time, traffic as well as weather parameters were measured. The photocatalytic activity was measured with a test reactor after a certain period of time. Based on that, a service interval was simulated to be approximately 13 months to always ascertain NO_x removal of at least 5%.

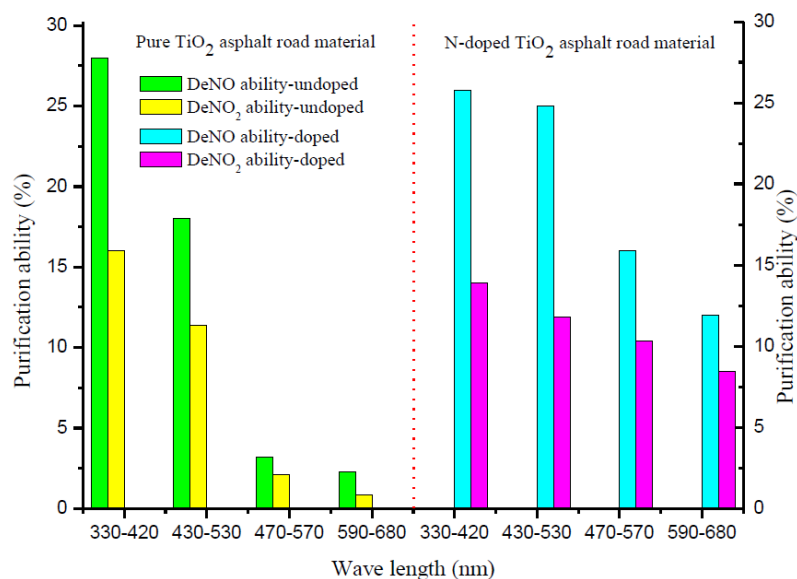


Figure 16. Degradation of NO and NO₂ on neat titania and N-doped titania coated asphalt under different irradiation conditions. (Reprinted/adapted with permission from Ref. [90]).

A comprehensive investigation on the reduction of the bacterial load on different surfaces with photocatalytic coatings under visible light was published by Krishna et al. [116]. They developed a titania based, bacteria-sensitized paint and confirmed the feasibility of the approach by describing and proving the underlying reaction mechanisms. By contacting anatase with a visible light absorbing contaminant, the photocatalytic activity was increased. The photocatalytic effect was further enhanced by incorporating polyhydroxy fullerenes into the material. It was shown that *Staphylococcus aureus* was inactivated on the (modified) TiO₂ coating. Furthermore, Krishna et al. coated multiple objects in a beta facility, i.e., wall (W), thermostat (T), locker (L), knob (K), soap dispenser (D), bathroom rail (R), bed rail (B), and kitchen counter (C), with the BioShield NuTiO paint as ground layer and an antimicrobial layer on top. After that, they counted the bacterial load multiple times for 12 months (Figure 17). The initial bacterial burden of W and T were underneath a concentration that could be harmful. The initial number of bacteria on the surfaces of L, K, R, B, and C exceeded the harmless concentration. The initial bacterial load of D was lower than the harmless concentration, possibly due to a disinfectational effect of the soap agents used in the soap dispenser. At surfaces of T, W, L, K, R and B, removal of the bacteria burden up to 99% was observed. At C, the number of bacteria remained at a harmful level. This was possibly due to mechanical abrasion of photocatalytic paint during cleaning this surface. It was observed, that coating with a rutile ground layer and anatase top layer performed better than an anatase/anatase coating.

Lettieri et al. particularly addressed the ageing effects of photocatalysts under natural conditions [111]. For this purpose, they prepared titania sol spray coated limestones and aged them in an urban area on a rooftop for 1 year. The photocatalytic activity has been tracked via Rhodamine B degradation at aged limestones. It was shown that the freshly coated sample had the fastest degradation kinetics and the highest degradation efficiency (92%) after 7.5 h in contact with Rhodamine B. After 8 and 12 months of ageing, degradation kinetics were slower and degradation efficiency was reduced to 74 and 76%, respectively. As a reference, the degradation efficiency of uncoated limestone was 72%. After washing off the surface, the subsequent degradation test showed a higher degradation efficiency of 85% for 12 months aged coated limestone. These results indicate both ablation of TiO₂ and deactivation of active surface states during ageing.

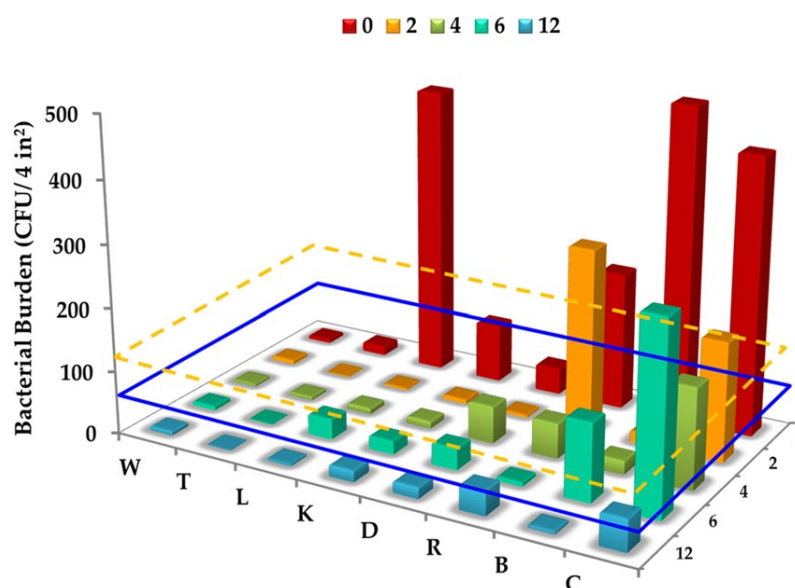


Figure 17. Bacterial load on wall (W), thermostat (T), locker (L), knob (K), soap dispenser (D), bathroom rail (R), bed rail (B), and kitchen counter (C) coated with polyhydroxy fullerenes containing anatase; initial concentration, and 2, 4, 6 and 12 months after coating. Also counts of harmless level (blue line) and counts of bacteria on an average clinical copper surface (yellow dotted line) are shown. (Reprinted/adapted with permission from Ref. [116]).

Colangiuli et al. investigated ageing effects of titania nanoparticles in fluoropolymer coated on limestone in the same environment as aforementioned by Lettieri et al. over medium to long-term runs. Titania based hydrophobic fluoropolymer coated limestones were aged for one year. After a certain time, the self-cleaning efficiency of the surface was characterized via decoloration of Rhodamine B. Overall, the authors observed a loss of photocatalytic activity during 1 year of ageing like observed by Lettieri before. The loss was possibly due to the low ability of the polymer to hold nanoparticles on its surface. Moreover, the authors pointed out that coupling of nanoparticles and fluoropolymer leads to adsorption of water soluble ions on the nanoparticles' surface, which possibly leads to a damage of the stone [119].

Fan et al. investigated a C-modified titania asphalt for air purification in both laboratory and field scale studies [123]. The photocatalyst nanoparticles were spray coated onto a bitumen surface. For a laboratory scale test, P25 and synthesized photocatalyst particles with different loading were spray coated onto asphalt and photocatalytic NO_x degradation was tracked in a test chamber. After 3 h, approximately 50% of NO_x was degraded, whereas with C-TiO₂ (1 mg m⁻²) NO_x was completely degraded after only 1.5 h. For real on-site tests, half of a model road was coated in the same manner as in the laboratory scale test and radiated with real sunlight. The NO_x concentration was measured during the experiments. It was shown that NO_x concentration above the coated asphalt was always lower than above the uncoated one.

Photocatalytic degradation of NO and toluene with Mn-doped titania in wall painting was measured by Maggos et al. [92]. Their aim was to reduce the aforementioned pollutants in indoor air in a medical building. The degradation was measured in both laboratory scale and real scale indoor rooms under visible light. The photocatalyst was dispersed in a paint. For the real scale measurement, the paint was applied in a 120 m² room and compared to an unpainted reference room. In laboratory tests, the photocatalyst exhibited a higher removal of NO and toluene (60 and 16%) than in the real scale test (NO: 19%; toluene: 5%). The higher degradation efficiency in laboratory scale was explained by diverse effects such as temperature, relative humidity, wind speed, and light intensity. In addition, the authors interpreted the higher removal of NO compared to toluene in terms of intrinsic properties of the gas and the chemical behavior of titania particles.

Šuligoj et al. studied the properties of Zr-modified $\text{TiO}_2/\text{SiO}_2$ films on glass [23]. After spray coating onto glass, self-cleaning and anti-fogging properties were tested for 20 months under realistic practical conditions. It was shown that no apparent self-cleaning ability was present in contrast to previous laboratory tests. However, the anti-fogging property could be proven (Figure 18).



Figure 18. Antifogging effect of uncoated and TiZr coated glass. (Reprinted/adapted with permission from Ref. [23]).

Villard de Oliveira et al. investigated the CVD of Ti-Cu-O and TiO_2 films on glass and their applicability for antibiofouling layers in marine environments [82]. In particular, they used aerosol-assisted metal organic chemical vapor deposition with different compositions of Ti-cations and Cu-cations (3-to-1 called 16TiCuO and 1-to-1 called 58TiCuO). It was found that TiO_2 forms microflowers upon deposition, while Ti-Cu-O films exhibit reasonably flat structures. Moreover, layers coated onto polycarbonate were tested in real seawater. After 10, 17, 25, and 38 days, samples were taken and the percentage of the coverage with cells and diatoms was estimated. After approximately 10 days, every sample still exhibited a low coverage with diatoms. After 25 days, samples with TiO_2 -microflowers had a 32% coverage whereas the samples 16TiCuO and 58TiCuO were characterized by a 43 and 82% coverage, respectively. After 38 days, the coverage of TiO_2 -microflowers, 16TiCuO, and 58TiCuO was 40, 66 and 95%, respectively. Additionally, multiple samples were covered with *Phaeodactylum tricornutum* and *Navicula perminuta* as model diatoms for understanding the dependence of the size of microorganism and the space between microflowers. It was shown that the diatoms are stronger adhered to the surface if the space between the flowers is the same as the size of the diatoms, whereas the diatoms are less adhered when the space between the TiO_2 -microflowers is larger than the size of the diatoms. In conclusion, TiO_2 as well as TiO_2 -Cu showed a sufficient removal of foulings on the surface, which makes these materials promising candidates in antifouling applications.

60 m of a street surface in Alcobendas (Community of Madrid, Spain) were coated with commercially available photocatalytic dispersion via spray coating (Figure 19) [108]. In this field study, Fernández-Pampillón et al. wanted to track NO_x degradation in real urban areas during a 41 days time period. The paint used showed in a laboratory scale a high photocatalytic activity. In summary, the group did not observe any degradation of NO_x in the observed area during their measurement campaign. They suggested three possible reasons: high volume-to-surface-ratio, low speed of transporting NO_x molecules to active surface states, and the low deposition rate of NO_x in comparison with high emission flows.

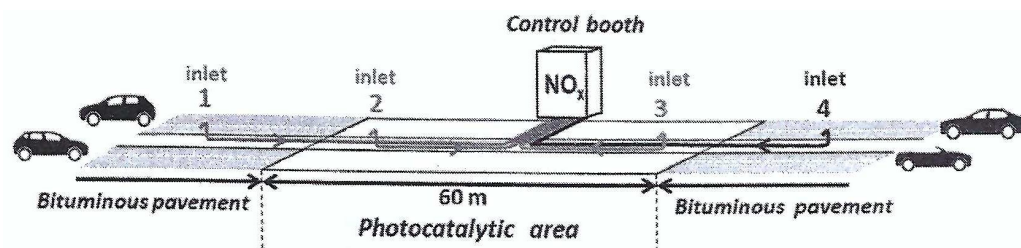


Figure 19. Illustration of the experimental setup for a real-scale test of a road surface coated with a photocatalyst for the removal of NO_x. (Reprinted/adapted with permission from Ref. [108]).

For biomedical applications, Geis-Gerstorfer et al. coated capillary tubes, silicon wafers, quartz crystals and model Ti implant surfaces with anatase layers prepared by reactive pulse magnetron sputtering. The photocatalytic behavior was studied upon the adsorption/desorption and the decomposition of human serum albumin (HSA). Therefore, they used quartz crystals as acoustic mass-sensitive sensors in a microbalance system. After the onset of albumin flow the protein adsorbed on the modified quartz crystals and caused a decrease in the frequency. If the sample was irradiated with UV, the frequency for the anatase film increased gradually, while it stayed the same for pure Ti. After four UV treatments, only 24% of the previously adsorbed protein mass remained on the anatase surface. This suggests that almost all of the adsorbed HSA has been degraded [117].

4.3. Water Purification

Moustakas et al. developed an ultrafiltration membrane coated with nanostructured TiO₂ for combined visible light photocatalysis and ultrafiltration [98]. The membrane was dipped into a sol of titania and after tempering it was put into the filtration reactor (Figure 20). This prototype was used for discoloration and filtration of methyl orange and methylene blue dye in water under both UV and visible light. Depending on flow rate, light source, and targeted molecule, the degradation was quite efficient. Overall, the group concluded that the coated external surface of the membrane avoids fouling, whereas the coated inner surface of the membrane provides better photocatalytic degradation due to higher mass per water volume ratio. Moreover, the highly asymmetric pore structure of the membranes used caused turbulences which led to increased mixing and longer contact time of the pollutants with the inner photocatalyst.

Zhao et al. tried to reduce harmful loads of carbon-bacteria complexes in drinking water [99]. For that, they built a pilot scale reactor based on a nanostructured titania film. During a 5 day test trial, the inactivation efficiency of bacteria was as high as 100%. The concentration of harmful bacteria in effluent water was below the Chinese limit for drinking water.

Yu et al. constructed another pilot scale reactor for photocatalytic purification of water [89]. The reactor consisted of a pipe containing a helically structured support (Figure 21). The stainless steel support material was first dip coated with silica and then sprayed with P25 titania nanoparticles. The helical support was placed inside an annular reactor. The disinfection activity was tested by deactivation of *E. coli* (Figure 22) under UV radiation with photocatalyst, under UV irradiation without photocatalyst (UV treatment), and with photocatalyst but without UV radiation (adsorption test). The combined UV irradiation and photocatalyst system showed the highest depolluting effect.

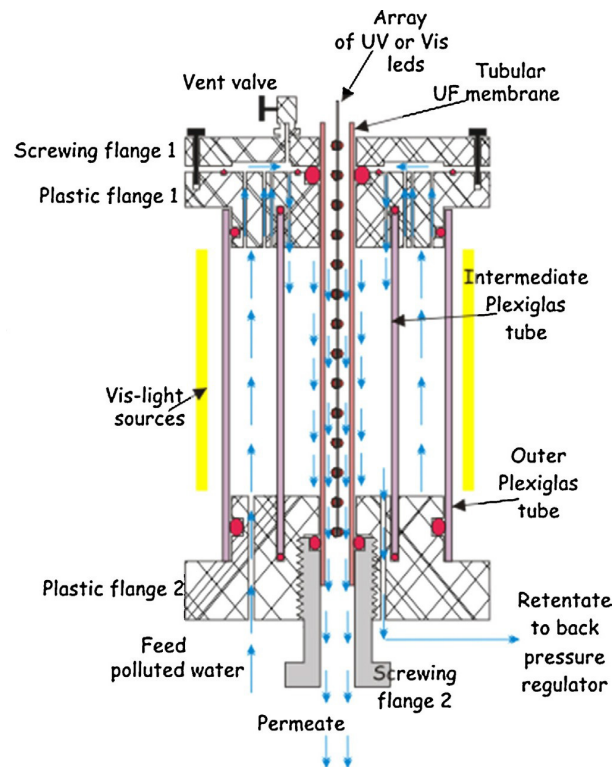


Figure 20. Illustration of a membrane reactor with photocatalytic support for combined visible light photocatalysis and ultrafiltration. (Reprinted/adapted with permission from Ref. [98]).

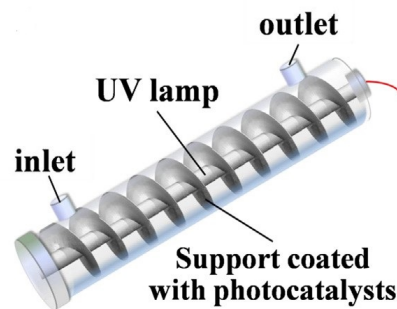


Figure 21. Photocatalyst coated, helical structure by Yu et al. for water purification. (Reprinted/adapted with permission from Ref. [89]).

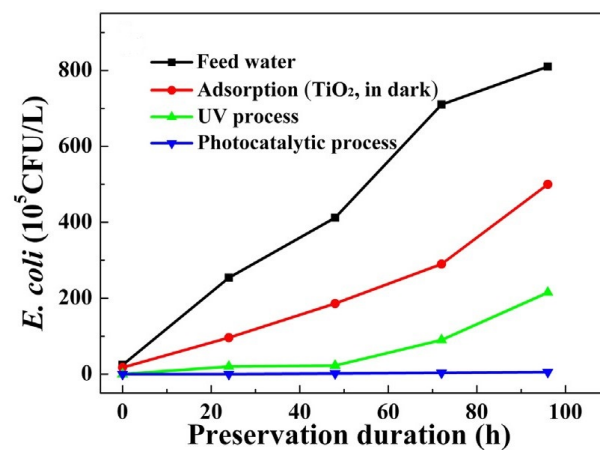


Figure 22. Colony forming units of *E. coli* during several hours of water purification with the reactor developed by Yu et al. (Reprinted/adapted with permission from Ref. [89]).

Saran et al. investigated a thin film plate reactor with Ag-doped titania. Their aim was to clean wastewater of a sugar refinery (Figure 23) [115]. Silver was reduced onto TiO₂ nanoparticles which were spray coated onto ceramic floor tiles. Tiles coated with neat TiO₂ particles and uncoated tiles served as reference samples. The tiles were put into sunlight, and waste water was circularly pumped over them. Moreover, the effect of additional parameters such as flow rate, pH value, and added H₂O₂ were studied. After 8 h of solar irradiation, the chemical oxygen demand (COD) for water treated with Ag-TiO₂, neat TiO₂, and uncoated tile was 95, 86 and 22%, respectively. With optimal parameters for flow rate, pH value, and H₂O₂, the COD could be reduced by 99% after 3 h of solar irradiation. After ten cleaning cycles, a 22% decrease in degradation efficiency was observed. This was possibly due to ablation of the catalyst or blockage of the active surface. The authors concluded that such Ag-TiO₂ reactors are a very effective method for wastewater treatment of sugar refineries.

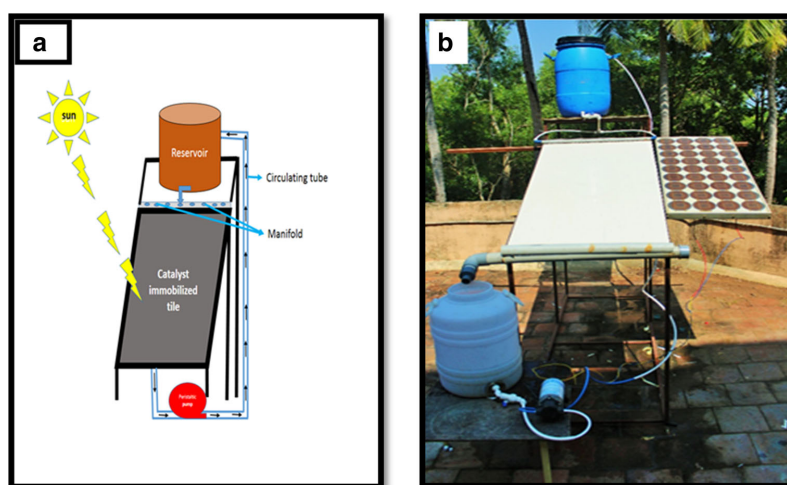


Figure 23. Scheme (a) and built prototype (b) of a thin film plate reactor for purifying sugar refinery wastewater. (Reprinted/adapted with permission from Ref. [115]).

Saran et al. designed a fixed bed tubular reactor (Figure 24) based on silver-doped TiO₂ and tested it for the treatment of rainwater [114]. First, they treated tap water with *E. coli*, MS-2 phage, and spores of *aspergillus niger*. This tap water was passed through the reactor under sunlight. Undoped titanium dioxide, an uncoated reactor, and the corresponding dark samples served as reference. *E. coli* was degraded with doped and undoped TiO₂ after 30 and 45 min, respectively. MS2-phage was inactivated after 60 (doped) and 90 min (undoped), respectively. *Aspergillus niger* was degraded fully after 90 min with doped TiO₂. 60% of the bacteria were inactivated after 120 min with undoped TiO₂. The corresponding dark samples showed no or only slight antibacterial effect. *E. Coli* was degraded faster than MS-2 phage and that faster than *Aspergillus niger*. The reason given by the authors was the different structure of the bacteria strains. Subsequently, the purification of rainwater was tested. After 120 min (undoped) and 90 min (doped), the bacteria were completely inactivated, but the degradation was slower than in the previously mentioned tests. The authors explained this by possible additional organic impurities. After repeated use, only a slight decrease in photocatalytic activity was observed, which could be explained by decomposition of the catalyst or by other experimental effects.



Figure 24. Fixed-bed tubular reactor for purification of rainwater. (Reprinted/adapted with permission from Ref. [114]).

Mahy et al. focused their research on the treatment of municipal and industrial water by means of oxidation processes [109]. They compared oxidation by ozone, photolysis, and photocatalysis. First, they prepared a silver-doped titanium dioxide and dip coated it onto a glass. On a laboratory scale, they tested different concentrations of silver and titanium dioxide ratios. The photocatalytic properties were tested using several typical impurities in water. The best result was achieved with a catalyst consisting of 2 wt% silver and 10 wt% P25. In addition, coating by spray and dip coating was compared. Spray coating was characterized as cheaper, more flexible and easier for scale-up in particular for larger components. The group spray coated in a second approach the catalyst onto stainless steel and placed it in a 200 l prototype water purifier. It could be shown that 4 impurities were removed directly by ozone within 30 min. 3 impurities were just removed by photolysis. 5 further impurities were removed by photocatalysis only. In summary, the purification by various oxidation processes turned out to be a good choice to clean water samples. The degradation of some molecules was only possible through certain purification processes.

Based on these findings, Mahy et al. developed a combined reactor of ozonation, UV illuminated photocatalysis, and active carbon filter for wastewater treatment [91]. This reactor was tested at laboratory, pilot, and industrial scales. The same photocatalytic material was used as in the previously presented work [109]. At laboratory scale, photocatalytic activity was demonstrated using 22 different impurities. At pilot scale, the photocatalytic material was sprayed on the inside of a cylindrical steel reactor. Ozonation was implemented as well. The degradation of pollutants was investigated on different water samples: water from the laboratory test with 22 contaminants, two industrial wastewater samples (textile company and culture media company), and municipal wastewater. As a result, 16 of the 22 contaminants were completely degraded and the remaining components were partially removed. The water from the textile company was toxic before and after treatment. The other initially toxic industrial wastewater was non-toxic after the treatment. The municipal wastewater was non-toxic due to its previous treatment in a wastewater treatment plant. On an industrial scale, the water purifying system was used as a tertiary treatment in a real wastewater treatment plant. Here, the treatment plant additionally consisted of an active carbon filter. With the combined technology, a purification of more than 95% was achieved. The UV intensity and the flow rate were identified as decisive factors for a successful treatment of the wastewater.

Özkal et al. investigated the influence of a thin film parallel plate photocatalytic reactor on the degradation of different strains of bacteria under UV illumination. [64,129]. Degradation efficiency was dependent on initial bacteria concentration. It was shown that natural strains of *E. coli* were characterized by a lower degradation than artificial strains possibly due to protein structure. The degradation efficiency of gram(−) was lower than

that of gram(+) due to a more complex cell structure. The photocatalysis may support the degradation of antibiotic resistant bacteria.

Fazzani et al. incorporated ceramicized tissue into a pilot scale photoreactor (Figure 25) and investigated the water purification using the degradation of Rhodamine B under both UV and visible light [87]. Different TiO₂ photocatalysts (TACR and SiO₂:TiO₂) and different fabrics (SP, SC, C, SM) were tested. The two photocatalysts were an acidic TiO₂ nanoparticle suspension (TAC) diluted with DI water (TACR) and the TACR mixed with a silica sol and DI water (SiO₂:TiO₂). The different fabrics consisted of 6% cotton/35% polyester with two different densities (SP und SC) and 100% cotton (C). For SM, no composition was available. The meshes were coated via dip coating. It was shown that the degradation was dependent on the selected parameters (Tables 4 and 5). The authors mentioned that further measurements with a larger reactor type were still pending.

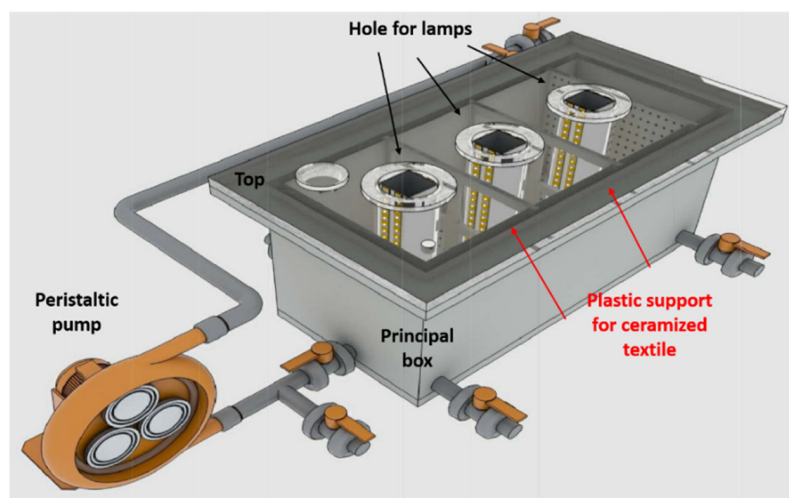


Figure 25. Photocatalytic ceramicized tissue based water purifying reactor according to Fazzani et al. (Reprinted/adapted with permission from Ref. [87]).

Table 4. Photocatalytic efficiency of ceramicized tissues with different photocatalytic coatings under visible light and UV irradiation. (Reprinted/adapted with permission from Ref. [87]).

Irradiation Light	Coating	Photocatalytic Efficiency %
Visible	TACR	49
Visible	TiO ₂ :SiO ₂	51
UV	TACR	64
UV	TiO ₂ :SiO ₂	60

Table 5. Photocatalytic efficiency of different coated ceramicized tissues under UV and visible light irradiation. (Reprinted/adapted with permission from Ref. [87]).

Fabric	Photocatalytic Efficiency % (UV LED)	Photocatalytic Efficiency % (Visible LED)
SP	49	64
SC	64	54
SM	65	61
C	67	57

An alumina-based photocatalyst-coated membrane for wastewater treatment was developed by Deeppracha et al. [96]. The membrane was dipped in an aqueous suspension of P25 and hectorite. The photocatalytic activity was then measured using methylene blue and phenol. In addition, the reduction of the permeate flow was investigated. It was found that 24% less water passed through the membrane after coating. However, an efficient

degradation of the impurities could be proven. The authors stated that the method should be well suited for larger reactors, too.

Dalanta et al. produced a polysulfone membrane with a Co-doped titanium dioxide/silicon dioxide composite [83]. This membrane was intended to be used for the photocatalytic treatment of petroleum refinery wastewater via filtration and UV light as well as for the removal of foulants on the surface. The membrane was produced via non-induced phase separation. As a reference, membranes with only SiO₂ (M-02), only TiO₂ (M-03), only Co/SiO₂ (M-04), only TiO₂@SiO₂ (M-05), with Co-TiO₂@SiO₂ (M-06), and without any particles (M-01) were prepared. Figure 26 depicts the degradation rates of COD, NH₃N, and phenol. M-06 exhibited the highest impurity degradation rate. Furthermore, the authors state that the addition of the Co-TiO₂@SiO₂ particles increased the porosity of the membrane and the mechanical stability, among other properties. In summary, the authors claimed a high photocatalytic activity, a pronounced self-cleaning effect of the membrane, and a high water-cleaning efficiency with UV light for their system.

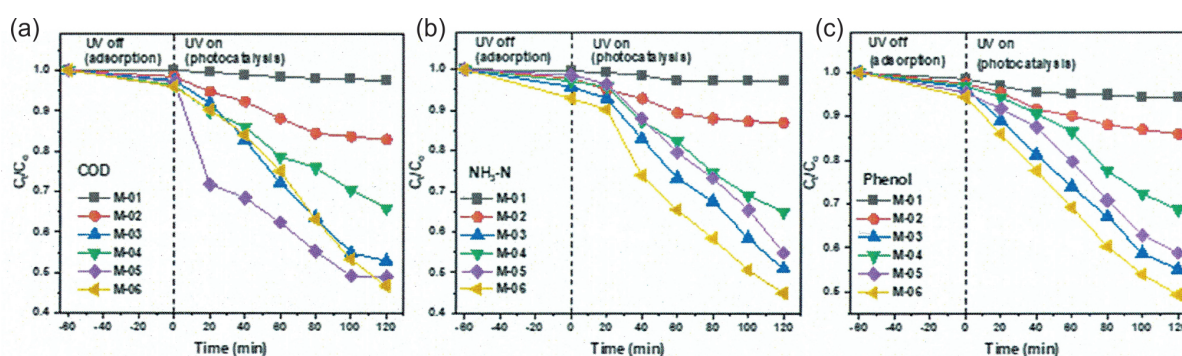


Figure 26. Concentration in relation to the initial concentration of COD (a), NH₃-N (b) and phenol (c) in petroleum refinery wastewater after purification with a photocatalytic membrane without and with UV irradiation. The different membranes were coated with only SiO₂ (M-02), only TiO₂ (M-03), only Co/SiO₂ (M-04), only TiO₂@SiO₂ (M-05), with Co-TiO₂@SiO₂ (M-06) and without any particles (M-01). (Reprinted/adapted with permission from Ref. [83]).

Porley and his team coated glass beads with Bi₄Ti₃O₁₂-TiO₂ (BTO-TiO₂) using an immersion technique [86]. The coated beads were intended to be used to purify water from Indian sources into drinking water using sunlight radiation. For the test, water from the various sources was stored in commercial drinking bottles with glass beads. Glass beads without catalyst and glass beads coated only with titanium dioxide served as reference. After 3 h, the authors did not observe any reduction in total suspended solids. It was shown that the untreated water tended to have the highest load of bacteria colony forming units (Figure 27). In contrast, bacteria degradation was highest with the BTO-TiO₂ catalyst, followed by the TiO₂ catalyst, followed by the setup without catalyst. However, a complete degradation was not achieved. The authors considered the large volume and the resulting mass transport effects as reasons, which could have been improved by moderate mixing.

Horváth et al. invented a water filter based on TiO₂ nanotubes and carbon nanotubes for the removal of bacteria, viruses, and organic matter under solar irradiation [84]. The structure used is shown in Figure 28. The TiO₂ nanotubes were fabricated via a heat treatment process. The carbon nanotubes were prepared via CVD. The final membranes were produced via doctor blading. Using a mixture of 9 different contaminants, the capability of the photocatalyst for contaminant removal was demonstrated. The solution was circularly pumped several times; at the beginning a decrease of gabapentin and metformin concentration of about 25% was observed. Subsequently, the concentration increased again due to thermal desorption before decreasing again, but to a smaller extent. The authors suggested that the reason for the weaker decrease was the shorter contact time of a weaker concentrated solution. Furthermore, the treatment of river water was tested. It was shown that bacteria were both mechanically retained and photocatalytically

inactivated. In the test, however, the degradation under UV light was stronger than under sunlight. According to Horváth et al. the reactor can be easily up-scaled by increasing the area of the filter.

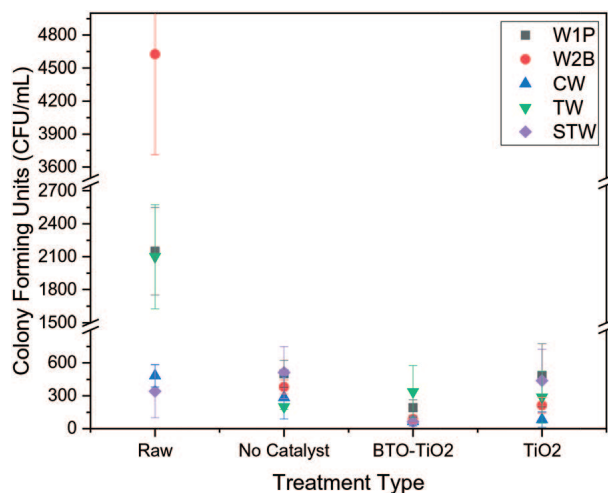


Figure 27. Colony forming units in water from different sources in India (W1P, W2B, CW, TW, STW) without treatment (raw), after 5 h of storage in a bottle in sunlight (no catalyst), and after treatment with (doped) photocatalytically active glass spheres (BTO-TiO₂ and TiO₂) for 5 h in a bottle in sunlight. (Reprinted/adapted with permission from Ref. [86]).

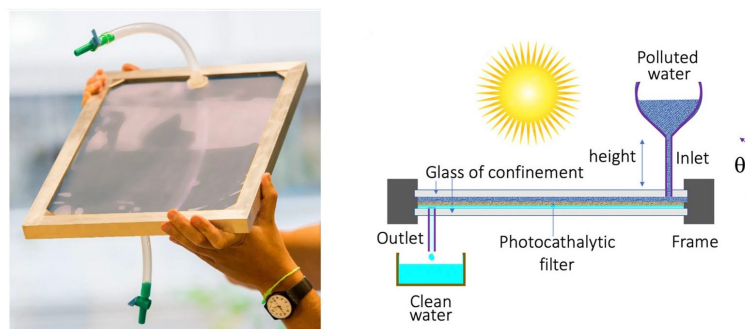


Figure 28. Picture and illustration of a photocatalytic water filter. (Reprinted/adapted with permission from Ref. [84]).

Faßauer et al. immobilized TiO₂ on a cellular ceramic for wastewater treatment. For this purpose, a ceramic foam with different pore sizes was coated with a TiO₂ suspension in an immersion process. The layer thickness of TiO₂ was up to 100 µm. It was observed that the formation of hydroxyl radicals was highest at medium pore sizes and lower flow rates. The authors mentioned that with a comparatively low energy input compared to other AOP-procedures (Advanced Oxidation Processes), complete degradation of pollutants such as carbamazepine and diclofenac with simultaneous disinfection is possible [120].

5. Standardized Methods and Protocols

There is not necessarily a lack of standardized methods and protocols for comparing the activity, efficiency, or long-term stability of photocatalytic materials. In catalytic air purification with semiconductors including photoactive building material a vast number of norms exist for the abatement of NO_(x) (for semiconducting materials: ISO 22197-1; for thin films and coatings: prEN 16980-1), formaldehyde (ISO 22197-4; under indoor lighting environments: ISO 17168-4), acetaldehyde (ISO 22197-2; under indoor lighting environments: ISO 17168-2 and ISO 19652 (for complete decomposition)), toluene (ISO 22197-3; under indoor lighting environments: ISO 17168-3), and methyl mercaptan (ISO 22197-5; under indoor lighting environments: ISO 17168-5). A standard protocol for the

measurement of the efficiency of complete photocatalytic devices used for the elimination of VOC and odor in indoor air can be found in norm EN 16846-1.

The investigation of the self-cleaning effect of photocatalytic surfaces has been standardized, e.g., within the norms ISO 10678 (methylene blue degradation), EN 1096-5 (coated glass surfaces), ISO 27448 (measurement of water contact angle), ISO 19810 (water contact angle under indoor lighting environments), EN 16845-1 (anti-soiling chemical activity using adsorbed organics), and ISO 21066 (reduction of resazurin in a deposited ink film).

Standard procedures to measure the antibacterial inactivation by photocatalytic semiconductors are given in ISO 27447 and in ISO 17094 (under indoor lighting conditions). The antiviral activity can be tested with norms ISO 18061 and ISO 18761 (under indoor lighting environments). The measurement of antifungal activity of photocatalytic materials is published in ISO 13125 and of antialgal activity in ISO 19635. A semi-dry method for estimating antibacterial activity on the actual environmental bacteria contamination surface is described in ISO 22551.

Additionally, for the photocatalytic treatment and purification of water samples standard procedures have been published in norms, e.g., EN 17120 (measurement of phenol degradation), ISO 22601 (phenol decomposition measurement by quantitative analysis of total organic carbon (TOC)), ISO 10676 (measurement of forming ability of active oxygen), and ISO 19722 (measurement of dissolved oxygen consumption).

Finally, the durability and long term stability of photocatalytic materials can be investigated by the application of specific accelerated stress tests and exposure to artificial harsh conditions, that are ideally close to real world scenarios. Procedures and protocols addressing these issues are, e.g., summarized in the norms EN ISO 4892-2 (artificial irradiating and weathering), DIN 52348 (abrasion and sand trickling test), or EN 927-3 (outdoor weathering test).

6. Conclusions and Outlook

Bases on our literature survey, the following main conclusions are drawn for the topics synthesis and preparation:

- Band gap engineering can be successfully accomplished by doping (or modification) with metals or non-metals. The absorption of visible light is most often explained by LSPR enhancement or intergap states.
- In addition, the intrinsic photoactivity sensitively depends on the level of doping. In ideal cases, charge carrier recombination is lower due to better charge separation. However, if the concentration of the dopant is too high, the photoactivity often decreases as dopants become recombination centers.
- For the coating of glass, walls, ceilings, streets, and other large surfaces, spray coating is the method of choice. Reasons are that spray coating is less expensive than most of the other alternatives, it can be more easily scaled up, and it is more flexible with respect to materials and preparation conditions as compared, e.g., to dip or spin coating.
- For smaller objects, dip and spin coating as well as impregnation and immersion can become useful. The two former methods allow a very precise adjustment of the layer thickness.
- Other preparation methods such as CVD, PVD or sputtering are rarely applied in real applications, since they usually demand expensive equipment, well defined surface geometries, and they need special coating precursors.
- In many cases, P25 or nanoparticles that are synthesized via the sol-gel-route are used as titania source. For this purpose, the sol, water or, e.g., a paint are used as a carrier material.
- In a few cases, TiO₂ is incorporated directly in the material. This is mainly the case with membranes and filters.
- The formation of anatase or rutile depends on the calcination temperature, time, and doping/modification technique.

During our research for already realized applications or developments in a prototype stage, we noticed the following main aspects:

- In the vast majority of published field or pilot scale tests, different building materials have been studied.
- Moreover, multiple tests have also been conducted in the field of air purifying systems. Here, some commercial systems are already available.
- In the field of water purification, industrial scale reactors are still rare. This is possibly because neither an efficient reactor system (fixed bed, flow through, coated concrete) nor a robust enough catalyst application technique (spray coating, dip coating, dispersion) could have been established for this purpose yet.
- Applications in medical fields such as implants are still niche applications. However, a number of studies could provide principal evidence that photocatalysts can effectively diminish the viral and bacterial load of air and surfaces in medical environments.
- Photocatalytic air purifiers are often used in combination with other technologies such as particle filters or plasma techniques.
- Photocatalytic air purification systems tested in realistic scenarios, such as coated walls and other surfaces in tunnels or on streets, very often exhibited a significant reduction in air purification efficiency as compared to laboratory scales. In some studies, there was even no effect at all verifiable. Reasons are probably the extremely high volume to catalyst surface ratio, the effect of temperature, relative humidity, other pollutants, the pollutant concentration, deactivation and ablation of titania, wind speed, contact as well as diffusion time. For air purifying purposes, the utilization of circulated air in combination with air purifiers is more promising to avoid some of the negative effects.
- Due to the low photocatalytic efficiency under visible light, most applications use artificial UV light from respective lamps. This is an additional cost factor and complicates the setting, but with energy-efficient UV-LED lamps it might be the best choice in many indoor and even outdoor applications.
- In general, many applications have been tested in pilot and especially in laboratory scale. However, field tests are very often missing to really evaluate the performance of the presented materials and systems. In the future, field studies should pay special attention to doped materials. These materials that could utilize a much larger part of the solar spectrum could become a show stopper for many outdoor applications.
- In most application studies, anatase is used as titania modification. However, there are hints that a combination of anatase and rutile layers or nanoparticles might be advantageous, probably due to enhanced charge carrier separation at the interface.
- Some studies focused on the long-term performance of the setups and the durability of the photocatalyst with regards to mechanical, optical, and catalytic properties under real conditions. However, it is consistently mentioned that more attention needs to be paid to this area in the future.

Multiple options for the analysis of the photocatalytic activity have been applied. We conclude that:

- In some studies, real pollutants such as NO_x, VOC, bacteria or other organic molecules in real environments were used.
- For most projects, especially for the test of prototypes, model pollutants or dyes are usually tested.
- It became also obvious that spectroscopic or electrochemical characterization of the photocatalyst (system) to deduce information such as, e.g., charge transfer efficiency, formed radicals and intermediate products, surface properties, photoquantum yields, catalyst morphology, turnover rates etc. in realistic environments are rare or even non-existent.

It became also evident that it is often very difficult to systematically compare many utilized photocatalytic materials and systems just on the basis of published data. Moreover, comparisons between photocatalytic and photoelectrochemical properties of a material are

rarely made. Since the charge carriers are measured directly using electrochemical methods, intrinsic charge transport properties can be determined directly under defined boundary surface conditions, whenever the photocatalytic coating material or thin film can be electrically contacted in an electrochemical cell. The knowledge of these intrinsic properties would help to better understand the influence of extrinsic effects on the performance of the whole photocatalytic system and probably enable improvements by rational design.

Deactivation is a further issue that needs to be much more addressed (already in earlier, more fundamental studies), since this is an extremely important and decisive factor for a later commercialization of the respective materials and systems. Therefore, many promising approaches that work well on the laboratory scale too often prove to be not robust enough for real world applications. Standardized long time and accelerated stress tests under realistic scenarios that can be run already in the laboratory could here much earlier allow to separate the wheat from the chaff. Obviously, there is still a lack of using standardized protocols for the quantitative assessment of the photocatalytic activity as described in many norms. This would—besides the intrinsic photocatalyst properties (see above)—help to assess the photocatalytic potential of many new or newly combined materials as early and as precise as possible. Nevertheless, even the best standard method can only approximately describe the full performance of the examined materials. Field tests will continue to be necessary.

Author Contributions: Conceptualization, M.E. and V.S.; writing—original draft preparation, S.T. and V.S.; writing—review and editing, M.E., S.T. and V.S.; visualization, S.T. and V.S.; supervision, M.E.; project administration, M.E. All authors have read and agreed to the published version of the manuscript.

Funding: M.E. and V.S. acknowledge funding from the Hightech Agenda of the Free State of Bavaria.

Institutional Review Board Statement: Not applicable.

Informed Consent Statement: Not applicable.

Data Availability Statement: Not applicable.

Conflicts of Interest: The authors declare no conflict of interest.

Abbreviations

The following abbreviations are used in this manuscript:

CB	Conduction Band
CFU	Colony Forming Unit
COD	Chemical Oxygen Demand
CPC	Compound Parabolic Reactor
CVD	Chemical Vapor Deposition
LSPR	Localized Surface Plasmon Resonance
PVD	Physical Vapor Deposition
SWCNT	Single wall carbon nanotube
TMiP	titanium mesh sheet modified with titania nanoparticles
TNT	Titania Nanotubes
TOBT	Tertoxybutyltitanate
TTIP	Titanium (IV) tetraisopropoxide
VB	Valence Band
VOC	Volatile Organic Compound

References

1. Birkett, M.; Dover, L.; Cherian Lukose, C.; Wasy Zia, A.; Tambuwala, M.M.; Serrano-Aroca, Á. Recent Advances in Metal-Based Antimicrobial Coatings for High-Touch Surfaces. *Int. J. Mol. Sci.* **2022**, *23*, 1162. [[CrossRef](#)] [[PubMed](#)]
2. Mohite, V.S.; Darade, M.M.; Sharma, R.K.; Pawar, S.H. Nanoparticle Engineered Photocatalytic Paints: A Roadmap to Self-Sterilizing against the Spread of Communicable Diseases. *Catalysts* **2022**, *12*, 326. [[CrossRef](#)]
3. Xu, X.; Yang, Y.; Liu, T.; Chu, B. Cost-effective Polymer-based Membranes for Drinking Water Purification. *Giant* **2022**, *10*, 100099. [[CrossRef](#)]

4. Abbass, K.; Qasim, M.Z.; Song, H.; Murshed, M.; Mahmood, H.; Younis, I. A review of the global climate change impacts, adaptation, and sustainable mitigation measures. *Environ. Sci. Pollut. Res.* **2022**, *29*, 42539–42559. [CrossRef]
5. Van Vliet, M.T.; Jones, E.R.; Flörke, M.; Franssen, W.H.; Hanasaki, N.; Wada, Y.; Yearsley, J.R. Global water scarcity including surface water quality and expansions of clean water technologies. *Environ. Res. Lett.* **2021**, *16*, 024020. [CrossRef]
6. Abedin, M.; Collins, A.E.; Habiba, U.; Shaw, R. Climate change, water scarcity, and health adaptation in southwestern coastal Bangladesh. *Int. J. Disaster Risk Sci.* **2019**, *10*, 28–42. [CrossRef]
7. Iervolino, G.; Zammit, I.; Vaiano, V.; Rizzo, L. Limitations and prospects for wastewater treatment by UV and visible-light-active heterogeneous photocatalysis: A critical review. *Heterog. Photocatal.* **2020**, *378*, 225–264. [CrossRef]
8. Negishi, N.; Chawengkijwanich, C.; Pimpha, N.; Larpiattaworn, S.; Charinpanitkul, T. Performance verification of the photocatalytic solar water purification system for sterilization using actual drinking water in Thailand. *J. Water Process. Eng.* **2019**, *31*, 100835. [CrossRef]
9. Marcelino, R.B.; Amorim, C.C.; Ratova, M.; Delfour-Peyrethon, B.; Kelly, P. Novel and versatile TiO₂ thin films on PET for photocatalytic removal of contaminants of emerging concern from water. *Chem. Eng. J.* **2019**, *370*, 1251–1261. [CrossRef]
10. Yang, Y.; Lai, Q.; Mahmud, S.; Lu, J.; Zhang, G.; Huang, Z.; Wu, Q.; Zeng, Q.; Huang, Y.; Lei, H.; et al. Photocatalytic antifouling membrane with dense nano-TiO₂ coating for efficient oil-in-water emulsion separation and self-cleaning. *J. Membr. Sci.* **2022**, *645*, 120204. [CrossRef]
11. Cabrera-Reina, A.; Martínez-Piernas, A.B.; Bertakis, Y.; Xekoukoulotakis, N.P.; Agüera, A.; Pérez, J.A.S. TiO₂ photocatalysis under natural solar radiation for the degradation of the carbapenem antibiotics imipenem and meropenem in aqueous solutions at pilot plant scale. *Water Res.* **2019**, *166*, 115037. [CrossRef] [PubMed]
12. Rueda-Márquez, J.J.; Palacios-Villarreal, C.; Manzano, M.; Blanco, E.; del Solar, M.R.; Levchuk, I. Photocatalytic degradation of pharmaceutically active compounds (PhACs) in urban wastewater treatment plants effluents under controlled and natural solar irradiation using immobilized TiO₂. *Sol. Energy* **2020**, *208*, 480–492. [CrossRef]
13. Hay, S.O.; Obee, T.; Luo, Z.; Jiang, T.; Meng, Y.; He, J.; Murphy, S.C.; Suib, S. The viability of photocatalysis for air purification. *Molecules* **2015**, *20*, 1319–1356. [CrossRef] [PubMed]
14. Huang, Y.; Ho, S.S.H.; Lu, Y.; Niu, R.; Xu, L.; Cao, J.; Lee, S. Removal of indoor volatile organic compounds via photocatalytic oxidation: A short review and prospect. *Molecules* **2016**, *21*, 56. [CrossRef] [PubMed]
15. Giampiccolo, A.; Tobaldi, D.M.; Leonardi, S.G.; Murdoch, B.J.; Seabra, M.P.; Ansell, M.P.; Neri, G.; Ball, R.J. Sol gel graphene/TiO₂ nanoparticles for the photocatalytic-assisted sensing and abatement of NO₂. *Appl. Catal. Environ.* **2019**, *243*, 183–194. [CrossRef]
16. Gallus, M.; Ciuraru, R.; Mothes, F.; Akylas, V.; Barmpas, F.; Beeldens, A.; Bernard, F.; Boonen, E.; Boréave, A.; Cazaunau, M.; et al. Photocatalytic abatement results from a model street canyon. *Environ. Sci. Pollut. Res.* **2015**, *22*, 18185–18196. [CrossRef]
17. Mahy, J.G.; Paez, C.A.; Hollevoet, J.; Courard, L.; Boonen, E.; Lambert, S.D. Durable photocatalytic thin coatings for road applications. *Constr. Build. Mater.* **2019**, *215*, 422–434. [CrossRef]
18. Gopalan, A.I.; Lee, J.C.; Saianand, G.; Lee, K.P.; Sonar, P.; Dharmarajan, R.; Hou, Y.L.; Ann, K.Y.; Kannan, V.; Kim, W.J. Recent progress in the abatement of hazardous pollutants using photocatalytic TiO₂-based building materials. *Nanomaterials* **2020**, *10*, 1854. [CrossRef]
19. Verband der Mineralfarbenindustrie e.V. Photoactive Construction Materials. Available online: <https://www.vdmi.de/en/products/applied-photocatalysis/product-range/photoactive-construction-materials/> (accessed on 3 August 2022).
20. Kim, M.; Kim, H.; Park, J. Empirical NO_x Removal Analysis of Photocatalytic Construction Materials at Real-Scale. *Materials* **2021**, *14*, 5717. [CrossRef]
21. Linkous, C.A.; Carter, G.J.; Locuson, D.B.; Ouellette, A.J.; Slattery, D.K.; Smitha, L.A. Photocatalytic inhibition of algae growth using TiO₂, WO₃, and cocatalyst modifications. *Environ. Sci. Technol.* **2000**, *34*, 4754–4758. [CrossRef]
22. Wang, R.; Hashimoto, K.; Fujishima, A.; Chikuni, M.; Kojima, E.; Kitamura, A.; Shimohigoshi, M.; Watanabe, T. Light-induced amphiphilic surfaces. *Nature* **1997**, *388*, 431–432. [CrossRef]
23. Šuligoj, A.; Pliekhova, O.; Vodišek, N.; Mihelčič, M.; Surca, A.K.; Kunič, R.; Šubic, B.; Starman, J.; Ugovšek, A.; Lavrenčič Štangar, U. Field Test of Self-Cleaning Zr-Modified-TiO₂-SiO₂ Films on Glass with a Demonstration of Their Anti-Fogging Effect. *Materials* **2019**, *12*, 2196. [CrossRef] [PubMed]
24. Ochiai, T.; Ichihashi, E.; Nishida, N.; Machida, T.; Uchida, Y.; Hayashi, Y.; Morito, Y.; Fujishima, A. Field performance test of an air-cleaner with photocatalysis-plasma synergistic reactors for practical and long-term use. *Molecules* **2014**, *19*, 17424–17434. [CrossRef] [PubMed]
25. Maurer, D.L.; Koziel, J.A. On-farm pilot-scale testing of black ultraviolet light and photocatalytic coating for mitigation of odor, odorous VOCs, and greenhouse gases. *Chemosphere* **2019**, *221*, 778–784. [CrossRef]
26. Assadi, A.A.; Bouzaza, A.; Soutrel, I.; Petit, P.; Medimagh, K.; Wolbert, D. A study of pollution removal in exhaust gases from animal quartering centers by combining photocatalysis with surface discharge plasma: From pilot to industrial scale. *Chem. Eng. Process. Process. Intensif.* **2017**, *111*, 1–6. [CrossRef]
27. Seiß, V.; Helbig, U.; Lösel, R.; Eichelbaum, M. Investigating and correlating photoelectrochemical, photocatalytic, and antimicrobial properties of TiO₂ nanolayers. *Sci. Rep.* **2021**, *11*, 22200. [CrossRef]
28. Villatte, G.; Massard, C.; Descamps, S.; Sibaud, Y.; Forestier, C.; Awitor, K.O. Photoactive TiO₂ antibacterial coating on surgical external fixation pins for clinical application. *Int. J. Nanomed.* **2015**, *10*, 3367. [CrossRef]

29. Wang, J.; Zhao, J.; Sun, L.; Wang, X. A review on the application of photocatalytic materials on textiles. *Text. Res. J.* **2015**, *85*, 1104–1118. [CrossRef]
30. Reid, M.; Whatley, V.; Spooner, E.; Nevill, A.M.; Cooper, M.; Ramsden, J.J.; Dancer, S.J. How does a photocatalytic antimicrobial coating affect environmental bioburden in hospitals? *Infect. Control. Hosp. Epidemiol.* **2018**, *39*, 398–404. [CrossRef]
31. Verhoeven, J.W. Glossary of terms used in photochemistry. *Pure Appl. Chem.* **1996**, *68*, 2223. [CrossRef]
32. Salomon, R.G. Homogeneous metal-catalysis in organic photochemistry. *Tetrahedron* **1983**, *39*, 485. [CrossRef]
33. Serpone, N.; Emeline, A.V. Suggested terms and definitions in photocatalysis and radiocatalysis. *Int. J. Photoenergy* **2002**, *4*, 91. [CrossRef]
34. Wang, Y.H.; Rahman, K.H.; Wu, C.C.; Chen, K.C. A review on the pathways of the improved structural characteristics and photocatalytic performance of titanium dioxide (TiO₂) thin films fabricated by the magnetron-sputtering technique. *Catalysts* **2020**, *10*, 598. [CrossRef]
35. Ge, M.; Cao, C.; Huang, J.; Li, S.; Chen, Z.; Zhang, K.Q.; Al-Deyab, S.; Lai, Y. A review of one-dimensional TiO₂ nanostructured materials for environmental and energy applications. *J. Mater. Chem.* **2016**, *4*, 6772–6801. [CrossRef]
36. Pelaez, M.; Nolan, N.T.; Pillai, S.C.; Seery, M.K.; Falaras, P.; Kontos, A.G.; Dunlop, P.S.; Hamilton, J.W.; Byrne, J.A.; O'shea, K.; et al. A review on the visible light active titanium dioxide photocatalysts for environmental applications. *Appl. Catal. Environ.* **2012**, *125*, 331–349. [CrossRef]
37. Luo, C.; Ren, X.; Dai, Z.; Zhang, Y.; Qi, X.; Pan, C. Present perspectives of advanced characterization techniques in TiO₂-based photocatalysts. *ACS Appl. Mater. Interfaces* **2017**, *9*, 23265–23286. [CrossRef] [PubMed]
38. Luttrell, T.; Halpegamage, S.; Tao, J.; Kramer, A.; Sutter, E.; Batzill, M. Why is anatase a better photocatalyst than rutile?—Model studies on epitaxial TiO₂ films. *Sci. Rep.* **2014**, *4*, 4043. [CrossRef]
39. Do, H.H.; Tran, T.K.C.; Ung, T.D.T.; Dao, N.T.; Nguyen, D.D.; Trinh, T.H.; Hoang, T.D.; Le, T.L.; Tran, T.T.H. Controllable fabrication of photocatalytic TiO₂ brookite thin film by 3D-printing approach for dyes decomposition. *J. Water Process. Eng.* **2021**, *43*, 102319. [CrossRef]
40. Nguyen, C.H.; Fu, C.C.; Juang, R.S. Degradation of methylene blue and methyl orange by palladium-doped TiO₂ photocatalysis for water reuse: Efficiency and degradation pathways. *J. Clean. Prod.* **2018**, *202*, 413–427. [CrossRef]
41. Hou, C.; Hu, B.; Zhu, J. Photocatalytic degradation of methylene blue over TiO₂ pretreated with varying concentrations of NaOH. *Catalysts* **2018**, *8*, 575. [CrossRef]
42. Gryparis, C.; Krasoudaki, T.; Maravelaki, P.N. Self-Cleaning Coatings for the Protection of Cementitious Materials: The Effect of Carbon Dot Content on the Enhancement of Catalytic Activity of TiO₂. *Coatings* **2022**, *12*, 587. [CrossRef]
43. Matsunaga, T.; Tomoda, R.; Nakajima, T.; Wake, H. Photoelectrochemical sterilization of microbial cells by semiconductor powders. *FEMS Microbiol. Lett.* **1985**, *29*, 211–214. [CrossRef]
44. Eichelbaum, M.; Seiß, V. Analysis of photoactive titanium dioxide layers: Common features and differences between photocatalysis and photoelectrochemistry. *Wiley Anal. Sci. Mag.* **2022**, *3*, 45–52.
45. Marques, A.C.; Rojas-Hernandez, R.E.; Almeida, R.M. Optical spectroscopy methods for the characterization of sol—Gel materials. *J. Sol-Gel Sci. Technol.* **2021**, *100*, 1–43. [CrossRef]
46. Ho, C.C.; Kang, F.; Chang, G.M.; You, S.J.; Wang, Y.F. Application of recycled lanthanum-doped TiO₂ immobilized on commercial air filter for visible-light photocatalytic degradation of acetone and NO. *Appl. Surf. Sci.* **2019**, *465*, 31–40. [CrossRef]
47. Miličević, N.; Novaković, M.; Potočnik, J.; Milović, M.; Rakočević, L.; Abazović, N.; Pjević, D. Influencing surface phenomena by Au diffusion in buffered TiO₂-Au thin films: Effects of deposition and annealing processing. *Surfaces Interfaces* **2022**, *30*, 101811. [CrossRef]
48. Fraunhofer. Sauber durch Sonnenkraft. Available online: <https://www.light-and-surfaces.fraunhofer.de/en/Press-Events/Press-2018/Press-Release-1-8-2018.html> (accessed on 6 August 2022).
49. Liu, Y.; Huang, J.; Feng, X.; Li, H. Thermal-sprayed photocatalytic coatings for biocidal applications: A review. *J. Therm. Spray Technol.* **2021**, *30*, 1–24. [CrossRef]
50. Krakowiak, R.; Musiał, J.; Bakun, P.; Spychała, M.; Czarczynska-Goslinska, B.; Mlynarczyk, D.T.; Koczorowski, T.; Sobotta, L.; Stanisław, B.; Goslinski, T. Titanium Dioxide-Based Photocatalysts for Degradation of Emerging Contaminants including Pharmaceutical Pollutants. *Appl. Sci.* **2021**, *11*, 8674. [CrossRef]
51. Ghosh, S.; Patra, R.; Majumdar, D.; Sen, K. Developing scenario of titania-based building materials for environmental remediation. *Int. J. Environ. Sci. Technol.* **2021**, *18*, 2077–2102. [CrossRef]
52. Oberdörster, G.; Stone, V.; Donaldson, K. Toxicology of nanoparticles: A historical perspective. *Nanotoxicology* **2007**, *1*, 2–25. [CrossRef]
53. Yaqoob, A.A.; Parveen, T.; Umar, K.; Mohamad Ibrahim, M.N. Role of nanomaterials in the treatment of wastewater: A review. *Water* **2020**, *12*, 495. [CrossRef]
54. Lin, L.; Jiang, W.; Chen, L.; Xu, P.; Wang, H. Treatment of produced water with photocatalysis: Recent advances, affecting factors and future research prospects. *Catalysts* **2020**, *10*, 924. [CrossRef]
55. Aruna, S.; Vismaya, A.; Balaji, N. Photocatalytic behavior of titania coatings fabricated by suspension and solution precursor plasma spray processes. *Mater. Manuf. Process.* **2021**, *36*, 868–875. [CrossRef]
56. Dell'Edera, M.; Porto, C.L.; de Pasquale, I.; Petronella, F.; Curri, M.L.; Agostiano, A.; Comparelli, R. Photocatalytic TiO₂-based coatings for environmental applications. *Catal. Today* **2021**, *380*, 62–83. [CrossRef]

57. Angulo-Ibáñez, A.; Aranzabe, E.; Beobide, G.; Castillo, O.; Goitandia, A.M.; Pérez-Yáñez, S.; Villamayor, A. Slot-Die Process of a Sol–Gel Photocatalytic Porous Coating for Large-Area Fabrication of Functional Architectural Glass. *Catalysts* **2021**, *11*, 711. [CrossRef]
58. Li, Z.; Wang, S.; Wu, J.; Zhou, W. Recent progress in defective TiO₂ photocatalysts for energy and environmental applications. *Renew. Sustain. Energy Rev.* **2022**, *156*, 111980. [CrossRef]
59. Nasr, M.; Eid, C.; Habchi, R.; Miele, P.; Bechelany, M. Recent progress on titanium dioxide nanomaterials for photocatalytic applications. *ChemSusChem* **2018**, *11*, 3023–3047. [CrossRef]
60. Wang, J.; Wang, Z.; Wang, W.; Wang, Y.; Hu, X.; Liu, J.; Gong, X.; Miao, W.; Ding, L.; Li, X.; et al. Synthesis, modification and application of titanium dioxide nanoparticles: A review. *Nanoscale* **2022**, *14*, 6709–6734. [CrossRef]
61. Wu, M.C.; Lin, T.H.; Hsu, K.H.; Hsu, J.F. Photo-induced disinfection property and photocatalytic activity based on the synergistic catalytic technique of Ag doped TiO₂ nanofibers. *Appl. Surf. Sci.* **2019**, *484*, 326–334. [CrossRef]
62. Thunyasirion, C.; Sribenjalux, P.; Supothina, S.; Chuaybamroong, P. Enhancement of air filter with TiO₂ photocatalysis for mycobacterium tuberculosis removal. *Aerosol Air Qual. Res.* **2015**, *15*, 600–610. [CrossRef]
63. Saqlain, S.; Cha, B.J.; Kim, S.Y.; Ahn, T.K.; Park, C.; Oh, J.M.; Jeong, E.C.; Seo, H.O.; Kim, Y.D. Visible light-responsive Fe-loaded TiO₂ photocatalysts for total oxidation of acetaldehyde: Fundamental studies towards large-scale production and applications. *Appl. Surf. Sci.* **2020**, *505*, 144160. [CrossRef]
64. Özkal, C.B.; Mantzavinos, D.; Meriç, S. Photocatalytic activity based-optimization of TTIP thin films for E. coli inactivation: Effect of Mn and Cu dopants. *Catal. Today* **2017**, *280*, 86–92. [CrossRef]
65. Martínez-Montelongo, J.H.; Medina-Ramírez, I.E.; Romo-Lozano, Y.; Zapien, J.A. Development of a sustainable photocatalytic process for air purification. *Chemosphere* **2020**, *257*, 127236. [CrossRef]
66. Thakur, I.; Verma, A.; Örmeci, B. Inactivation of bacteria present in secondary municipal wastewater effluent using the hybrid effect of Fe–TiO₂ catalyst. *J. Clean. Prod.* **2022**, *352*, 131575. [CrossRef]
67. Chen, J.; Qiu, F.; Xu, W.; Cao, S.; Zhu, H. Recent progress in enhancing photocatalytic efficiency of TiO₂-based materials. *Appl. Catal. Gen.* **2015**, *495*, 131–140. [CrossRef]
68. Oros-Ruiz, S.; Zanella, R.; Prado, B. Photocatalytic degradation of trimethoprim by metallic nanoparticles supported on TiO₂-P25. *J. Hazard. Mater.* **2013**, *263*, 28–35. [CrossRef]
69. Dozzi, M.V.; Prati, L.; Canton, P.; Sellì, E. Effects of gold nanoparticles deposition on the photocatalytic activity of titanium dioxide under visible light. *Phys. Chem. Chem. Phys.* **2009**, *11*, 7171–7180. [CrossRef]
70. Low, J.; Cheng, B.; Yu, J. Surface modification and enhanced photocatalytic CO₂ reduction performance of TiO₂: A review. *Appl. Surf. Sci.* **2017**, *392*, 658–686. [CrossRef]
71. Choi, H.; Chen, W.T.; Kamat, P.V. Know thy nano neighbor. Plasmonic versus electron charging effects of metal nanoparticles in dye-sensitized solar cells. *ACS Nano* **2012**, *6*, 4418–4427. [CrossRef]
72. Hou, W.; Cronin, S.B. A Review of Surface Plasmon Resonance-Enhanced Photocatalysis. *Adv. Funct. Mater.* **2013**, *23*, 1612–1619. [CrossRef]
73. Ma, Y.; Zhang, X.t.; Guan, Z.s.; Cao, Y.a.; Yao, J.n. Effects of zinc (II) and iron (III) doping of titania films on their photoreactivity to decompose rhodamine B. *J. Mater. Res.* **2001**, *16*, 2928–2933. [CrossRef]
74. Tong, T.; Zhang, J.; Tian, B.; Chen, F.; He, D. Preparation of Fe³⁺-doped TiO₂ catalysts by controlled hydrolysis of titanium alkoxide and study on their photocatalytic activity for methyl orange degradation. *J. Hazard. Mater.* **2008**, *155*, 572–579. [CrossRef] [PubMed]
75. Di Valentin, C.; Pacchioni, G. Trends in non-metal doping of anatase TiO₂: B, C, N and F. *Catal. Today* **2013**, *206*, 12–18. [CrossRef]
76. Dozzi, M.V.; Sellì, E. Doping TiO₂ with p-block elements: Effects on photocatalytic activity. *J. Photochem. Photobiol. Photochem. Rev.* **2013**, *14*, 13–28. [CrossRef]
77. Appasamy, J.S.; Kurnia, J.C.; Assadi, M.K. Synthesis and evaluation of nitrogen-doped titanium dioxide/single walled carbon nanotube-based hydrophilic self-cleaning coating layer for solar photovoltaic panel surface. *Sol. Energy* **2020**, *196*, 80–91. [CrossRef]
78. Fan, W.; Chan, K.Y.; Zhang, C.; Leung, M.K. Advanced Solar Photocatalytic Asphalt for Removal of Vehicular NO_x. *Energy Procedia* **2017**, *143*, 811–816. [CrossRef]
79. Jiang, Q.; Hou, J.; Liu, J.; Fu, Y.; Liu, Y. Visible Photocatalysis of a Building Glass Coated with N-F-TiO₂/rGO. In *Proceedings of the 11th International Symposium on Heating, Ventilation and Air Conditioning (ISHVAC 2019), Harbin, China, 12–15 July 2019*; Wang, Z., Zhu, Y., Wang, F., Wang, P., Shen, C., Liu, J., Eds.; Springer: Singapore, 2020; pp. 181–190. [CrossRef]
80. Dineshran, R.; Subasri, R.; Somaraju, K.; Jayaraj, K.; Vedaprakash, L.; Ratnam, K.; Joshi, S.; Venkatesan, R. Biofouling studies on nanoparticle-based metal oxide coatings on glass coupons exposed to marine environment. *Colloids Surf. Biointerfaces* **2009**, *74*, 75–83. [CrossRef]
81. Krumdieck, S.; Miya, S.; Lee, D.; Davies-Talwar, S.; Bishop, C. Titania-based photocatalytic coatings on stainless steel hospital fixtures. *Phys. Status Solidi* **2015**, *12*, 1028–1035. [CrossRef]
82. Villardi de Oliveira, C.; Petitbois, J.; Fay, F.; Sanchette, F.; Schuster, F.; Alhoussein, A.; Chaix-Pluchery, O.; Deschanvres, J.L.; Jiménez, C. Marine antibiofouling properties of TiO₂ and Ti-Cu-O films deposited by aerosol-assisted chemical vapor deposition. *Coatings* **2020**, *10*, 779. [CrossRef]

83. Dalanta, F.; Kusworo, T.D.; Aryanti, N. Synthesis, characterization, and performance evaluation of UV light-driven Co-TiO₂@SiO₂ based photocatalytic nanohybrid polysulfone membrane for effective treatment of petroleum refinery wastewater. *Appl. Catal. Environ.* **2022**, *316*, 121576. [[CrossRef](#)]
84. Horváth, E.; Gabathuler, J.; Bourdieu, G.; Vidal-Revel, E.; Benthem Muñoz, M.; Gaal, M.; Grandjean, D.; Breider, F.; Rossi, L.; Sienkiewicz, A.; et al. Solar water purification with photocatalytic nanocomposite filter based on TiO₂ nanowires and carbon nanotubes. *NPJ Clean Water* **2022**, *5*, 10. [[CrossRef](#)]
85. Delnavaz, M.; Mahdian, S.S.; Boshagh, M.A. Economical and operational optimization of the enhanced titania photocatalytic activity by plasmonic effect for the treatment of real petrochemical wastewater. *Pet. Sci. Technol.* **2022**, *40*, 2525–2544. [[CrossRef](#)]
86. Porley, V.; Chatzisyneon, E.; Meikap, B.C.; Ghosal, S.; Robertson, N. Field testing of low-cost titania-based photocatalysts for enhanced solar disinfection (SODIS) in rural India. *Environ. Sci. Water Res. Technol.* **2020**, *6*, 809–816. [[CrossRef](#)]
87. Faccani, L.; Ortelli, S.; Blosi, M.; Costa, A.L. Ceramized Fabrics and Their Integration in a Semi-Pilot Plant for the Photodegradation of Water Pollutants. *Catalysts* **2021**, *11*, 1418. [[CrossRef](#)]
88. Thuy, N.T.; May, D.T.; Thao, D.N.P.; Thuy, V.T.T.; Thanh, D.V.; Thanh, N.T.; Huy, N.N. Field study of visitors' behavior in incense burning and its induced air pollution assessment and treatment. *Environ. Sci. Pollut. Res.* **2022**, *29*, 45933–45946. [[CrossRef](#)]
89. Yu, H.; Song, L.; Hao, Y.; Lu, N.; Quan, X.; Chen, S.; Zhang, Y.; Feng, Y. Fabrication of pilot-scale photocatalytic disinfection device by installing TiO₂ coated helical support into UV annular reactor for strengthening sterilization. *Chem. Eng. J.* **2016**, *283*, 1506–1513. [[CrossRef](#)]
90. Chen, M.; Baglee, D.; Chu, J.W.; Du, D.; Guo, X. Photocatalytic oxidation of NO_x under visible light on asphalt pavement surface. *J. Mater. Civ. Eng.* **2017**, *29*, 1. [[CrossRef](#)]
91. Mahy, J.G.; Wolfs, C.; Vreuls, C.; Drot, S.; Dircks, S.; Boergers, A.; Tuerk, J.; Hermans, S.; Lambert, S.D. Advanced oxidation processes for waste water treatment: From laboratory-scale model water to on-site real waste water. *Environ. Technol.* **2021**, *42*, 3974–3986. [[CrossRef](#)]
92. Maggos, T.; Binas, V.; Siaperas, V.; Terzopoulos, A.; Panagopoulos, P.; Kiriakidis, G. A promising technological approach to improve indoor air quality. *Appl. Sci.* **2019**, *9*, 4837. [[CrossRef](#)]
93. Monteiro, R.A.; Rodrigues-Silva, C.; Lopes, F.V.; Silva, A.M.; Boaventura, R.A.; Vilar, V.J. Evaluation of a solar/UV annular pilot scale reactor for 24 h continuous photocatalytic oxidation of n-decane. *Chem. Eng. J.* **2015**, *280*, 409–416. [[CrossRef](#)]
94. Abou Saoud, W.; Kane, A.; le Cann, P.; Gérard, A.; Lamaa, L.; Peruchon, L.; Brochier, C.; Bouzaza, A.; Wolbert, D.; Assadi, A.A. Innovative photocatalytic reactor for the degradation of VOCs and microorganism under simulated indoor air conditions: Cu-Ag/TiO₂-based optical fibers at a pilot scale. *Chem. Eng. J.* **2021**, *411*, 128622. [[CrossRef](#)]
95. Schnabel, T.; Dutschke, M.; Schuetz, F.; Hauser, F.; Springer, C. Photocatalytic air purification of polycyclic aromatic hydrocarbons: Application of a flow-through reactor, kinetic studies and degradation pathways. *J. Photochem. Photobiol. Chem.* **2022**, *430*, 113993. [[CrossRef](#)]
96. Deeppracha, S.; Atfane, L.; Ayril, A.; Ogawa, M. Simple and efficient method for functionalizing photocatalytic ceramic membranes and assessment of its applicability for wastewater treatment in up-scalable membrane reactors. *Sep. Purif. Technol.* **2021**, *262*, 118307. [[CrossRef](#)]
97. Rodrigues-Silva, C.; Monteiro, R.A.; Dezotti, M.; Silva, A.M.; Pinto, E.; Boaventura, R.A.; Vilar, V.J. A facile method to prepare translucent anatase thin films in monolithic structures for gas stream purification. *Environ. Sci. Pollut. Res.* **2018**, *25*, 27796–27807. [[CrossRef](#)] [[PubMed](#)]
98. Moustakas, N.; Katsaros, F.; Kontos, A.; Romanos, G.E.; Dionysiou, D.; Falaras, P. Visible light active TiO₂ photocatalytic filtration membranes with improved permeability and low energy consumption. *Catal. Today* **2014**, *224*, 56–69. [[CrossRef](#)]
99. Zhao, J.H.; Chen, W.; Zhao, Y.; Liu, C.; Liu, R. UV/TiO₂ photocatalytic disinfection of carbon-bacteria complexes in activated carbon-filtered water: Laboratory and pilot-scale investigation. *J. Environ. Sci. Health Part A* **2015**, *50*, 1274–1281. [[CrossRef](#)]
100. Parashar, M.; Shukla, V.K.; Singh, R. Metal oxides nanoparticles via sol-gel method: A review on synthesis, characterization and applications. *J. Mater. Sci. Mater. Electron.* **2020**, *31*, 3729–3749. [[CrossRef](#)]
101. Ola, O.; Maroto-Valer, M.M. Review of material design and reactor engineering on TiO₂ photocatalysis for CO₂ reduction. *J. Photochem. Photobiol. Photochem. Rev.* **2015**, *24*, 16–42. [[CrossRef](#)]
102. Ho, W. Efficient photocatalytic degradation of NO by ceramic foam air filters coated with mesoporous TiO₂ thin films. *Chin. J. Catal.* **2015**, *36*, 2109–2118. [[CrossRef](#)]
103. Assadi, A.A.; Palau, J.; Bouzaza, A.; Penya-Roja, J.; Martinez-Soriac, V.; Wolbert, D. Abatement of 3-methylbutanal and trimethylamine with combined plasma and photocatalysis in a continuous planar reactor. *J. Photochem. Photobiol. Chem.* **2014**, *282*, 1–8. [[CrossRef](#)]
104. Zadi, T.; Assadi, A.A.; Nasrallah, N.; Bouallouche, R.; Tri, P.N.; Bouzaza, A.; Azizi, M.M.; Maachi, R.; Wolbert, D. Treatment of hospital indoor air by a hybrid system of combined plasma with photocatalysis: Case of trichloromethane. *Chem. Eng. J.* **2018**, *349*, 276–286. [[CrossRef](#)]
105. Nguyen, N.H.; Wu, H.Y.; Bai, H. Photocatalytic reduction of NO₂ and CO₂ using molybdenum-doped titania nanotubes. *Chem. Eng. J.* **2015**, *269*, 60–66. [[CrossRef](#)]
106. Boonen, E.; Akylas, V.; Barmpas, F.; Boréave, A.; Bottalico, L.; Cazaunau, M.; Chen, H.; Daële, V.; de Marco, T.; Doussin, J.; et al. Construction of a photocatalytic de-polluting field site in the Leopold II tunnel in Brussels. *J. Environ. Manag.* **2015**, *155*, 136–144. [[CrossRef](#)] [[PubMed](#)]

107. Gallus, M.; Akylas, V.; Barmpas, F.; Beeldens, A.; Boonen, E.; Boréave, A.; Cazaunau, M.; Chen, H.; Daële, V.; Doussin, J.; et al. Photocatalytic de-pollution in the Leopold II tunnel in Brussels: NO_x abatement results. *Builld. Environ.* **2015**, *84*, 125–133. [[CrossRef](#)]
108. Fernández-Pampillón, J.; Palacios, M.; Núñez, L.; Pujadas, M.; Sanchez, B.; Santiago, J.L.; Martilli, A. NO_x depolluting performance of photocatalytic materials in an urban area—Part I: Monitoring ambient impact. *Atmos. Environ.* **2021**, *251*, 118190. [[CrossRef](#)]
109. Mahy, J.G.; Wolfs, C.; Mertes, A.; Vreuls, C.; Drot, S.; Smeets, S.; Dircks, S.; Boegers, A.; Tuerk, J.; Lambert, S.D. Advanced photocatalytic oxidation processes for micropollutant elimination from municipal and industrial water. *J. Environ. Manag.* **2019**, *250*, 109561. [[CrossRef](#)]
110. Pal, S.; Laera, A.M.; Licciulli, A.; Catalano, M.; Taurino, A. Biphase TiO₂ microspheres with enhanced photocatalytic activity. *Ind. Eng. Chem. Res.* **2014**, *53*, 7931–7938. [[CrossRef](#)]
111. Lettieri, M.; Colangiuli, D.; Masieri, M.; Calia, A. Field performances of nanosized TiO₂ coated limestone for a self-cleaning building surface in an urban environment. *Builld. Environ.* **2019**, *147*, 506–516. [[CrossRef](#)]
112. Calia, A.; Lettieri, M.; Masieri, M.; Pal, S.; Licciulli, A.; Arima, V. Limestones coated with photocatalytic TiO₂ to enhance building surface with self-cleaning and depolluting abilities. *J. Clean. Prod.* **2017**, *165*, 1036–1047. [[CrossRef](#)]
113. Ochiai, T.; Hoshi, T.; Slimen, H.; Nakata, K.; Murakami, T.; Tatejima, H.; Koide, Y.; Houas, A.; Horie, T.; Morito, Y.; et al. Fabrication of a TiO₂ nanoparticles impregnated titanium mesh filter and its application for environmental purification. *Catal. Sci. Technol.* **2011**, *1*, 1324–1327. [[CrossRef](#)]
114. Saran, S.; Arunkumar, P.; Devipriya, S. Disinfection of roof harvested rainwater for potable purpose using pilot-scale solar photocatalytic fixed bed tubular reactor. *Water Sci. Technol. Water Supply* **2018**, *18*, 49–59. [[CrossRef](#)]
115. Saran, S.; Kamalraj, G.; Arunkumar, P.; Devipriya, S. Pilot scale thin film plate reactors for the photocatalytic treatment of sugar refinery wastewater. *Environ. Sci. Pollut. Res.* **2016**, *23*, 17730–17741. [[CrossRef](#)] [[PubMed](#)]
116. Krishna, V.; Bai, W.; Han, Z.; Yano, A.; Thakur, A.; Georgieva, A.; Tolley, K.; Navarro, J.; Koopman, B.; Moudgil, B. Contaminant-activated visible light photocatalysis. *Sci. Rep.* **2018**, *8*, 1894. [[CrossRef](#)] [[PubMed](#)]
117. Rupp, F.; Haupt, M.; Klostermann, H.; Kim, H.S.; Eichler, M.; Peetsch, A.; Scheideler, L.; Doering, C.; Oehr, C.; Wendel, H.; et al. Multifunctional nature of UV-irradiated nanocrystalline anatase thin films for biomedical applications. *Acta Biomater.* **2010**, *6*, 4566–4577. [[CrossRef](#)]
118. Ochiai, T.; Hayashi, Y.; Ito, M.; Nakata, K.; Murakami, T.; Morito, Y.; Fujishima, A. An effective method for a separation of smoking area by using novel photocatalysis-plasma synergistic air-cleaner. *Chem. Eng. J.* **2012**, *209*, 313–317. [[CrossRef](#)]
119. Colangiuli, D.; Lettieri, M.; Masieri, M.; Calia, A. Field study in an urban environment of simultaneous self-cleaning and hydrophobic nanosized TiO₂-based coatings on stone for the protection of building surface. *Sci. Total. Environ.* **2019**, *650*, 2919–2930. [[CrossRef](#)]
120. Saft, F.; Heymer, H.; Adler, J.; Faßauer, B. *Photocatalytic Wastewater Treatment with Functionalized Cellular Ceramics*; Annual Report 14/15; Fraunhofer Institute for Ceramic Technologies and Systems IKTS: Hermsdorf, Germany, 2014; Volume 1, p. 77.
121. Lee, M.; Li, P.; Koziel, J.A.; Ahn, H.; Wi, J.; Chen, B.; Meirkhanuly, Z.; Banik, C.; Jenks, W.S. Pilot-scale testing of UV-A light treatment for mitigation of NH₃, H₂S, GHGs, VOCs, odor, and O₃ inside the poultry barn. *Front. Chem.* **2020**, *8*, 613. [[CrossRef](#)]
122. Maggos, T.; Bartzis, J.; Liakou, M.; Gobin, C. Photocatalytic degradation of NO_x gases using TiO₂-containing paint: A real scale study. *J. Hazard. Mater.* **2007**, *146*, 668–673. [[CrossRef](#)]
123. Fan, W.; Chan, K.Y.; Zhang, C.; Zhang, K.; Ning, Z.; Leung, M.K. Solar photocatalytic asphalt for removal of vehicular NO_x: A feasibility study. *Appl. Energy* **2018**, *225*, 535–541. [[CrossRef](#)]
124. Zhao, Y.K.; Sung, W.P.; Tsai, T.T.; Wang, H.J. Application of nanoscale silver-doped titanium dioxide as photocatalyst for indoor airborne bacteria control: A feasibility study in medical nursing institutions. *J. Air Waste Manag. Assoc.* **2010**, *60*, 337–345. [[CrossRef](#)]
125. Sung, W.; Tsai, T.; Wu, M.; Wang, H.; Surampalli, R. Removal of indoor airborne bacteria by nano-Ag/TiO₂ as photocatalyst: Feasibility study in museum and nursing institutions. *J. Environ. Eng.* **2011**, *137*, 163–170. [[CrossRef](#)]
126. Blondeau, P.; Abadie, M.O.; Durand, A.; Kaluzny, P.; Parat, S.; Ginestet, A.; Pugnet, D.; Tourreilles, C.; Duforestel, T. Experimental characterization of the removal efficiency and energy effectiveness of central air cleaners. *Energy Buill Environ.* **2021**, *2*, 1–12. [[CrossRef](#)]
127. Ehm, C.; Frohmüller, M.O.; Flassak, T.; Stephan, D. On-site reduction of nitrogen oxides at an emission hotspot using actively vented photocatalytic reactors in a highway tunnel. *SN Appl. Sci.* **2022**, *4*, 153. [[CrossRef](#)]
128. Gharaibeh, A.; Smith, R.H.; Conway, M.J. Reducing spread of infections with a Photocatalytic reactor—Potential applications in control of hospital *Staphylococcus aureus* and *Clostridioides difficile* infections and inactivation of RNA viruses. *Infect. Dis. Rep.* **2021**, *13*, 58–71. [[CrossRef](#)] [[PubMed](#)]
129. Özkal, C.B.; Venieri, D.; Gounaki, I.; Meric, S. Assessment of thin-film photocatalysis inactivation of different bacterial indicators and effect on their antibiotic resistance profile. *Appl. Catal. Environ.* **2019**, *244*, 612–619. [[CrossRef](#)]